Rap1 potentiates endothelial cell junctions by spatially controlling myosin II activity and actin organization

Koji Ando,[1,2] Shigetomo Fukuhara,[1] Takahiro Moriya,[2] Yutaro Obara,[2,3] Norimichi Nakahata,[2] and Naoki Mochizuki[1]

[1]Department of Cell Biology, National Cerebral and Cardiovascular Center Research Institute, Suita, Osaka 565-8565, Japan
[2]Department of Cellular Signaling, Graduate School of Pharmaceutical Sciences, Tohoku University, Aoba, Aramaki, Aoba-ku, Sendai 980-8578, Japan
[3]Department of Pharmacology, Yamagata University School of Medicine, Yamagata 990-9585, Japan

Reorganization of the actin cytoskeleton is responsible for dynamic regulation of endothelial cell (EC) barrier function. Circumferential actin bundles (CAB) promote formation of linear adherens junctions (AJs) and tightening of EC junctions, whereas formation of radial stress fibers (RSF) connected to punctate AJs occurs during junction remodeling. The small GTPase Rap1 induces CAB formation to potentiate EC junctions; however, the mechanism underlying Rap1-induced CAB formation remains unknown. Here, we show that myotonic dystrophy kinase–related CDC42-binding kinase (MRCK)-mediated activation of non-muscle myosin II (NM-II) at cell–cell contacts is essential for Rap1-induced CAB formation. Our data suggest that Rap1 induces FGD5-dependent Cdc42 activation at cell–cell junctions to locally activate the NM-II through MRCK, thereby inducing CAB formation. We further reveal that Rap1 suppresses the NM-II activity stimulated by the Rho–ROCK pathway, leading to dissolution of RSF. These findings imply that Rap1 potentiates EC junctions by spatially controlling NM-II activity through activation of the Cdc42–MRCK pathway and suppression of the Rho–ROCK pathway.

Introduction

Adherens junctions (AJs) constituted by cadherin family adhesion receptors are formed at cell–cell junctions in both endothelial cells (ECs) and epithelial cells, and are strengthened by the actin cytoskeleton to maintain tissue integrity. AJs mainly exist in two forms: stable linear AJs, also called zonula adherens, supported by circumferential actin bundles (CAB), which are defined as linear actin bundles that align along the cell–cell junctions; and dynamic punctate AJs connected by radial stress fibers (RSF; Ayollo et al., 2009; Millán et al., 2010; Taguchi et al., 2011; Hoelzle and Svitkina, 2012; Huveneers et al., 2012). In the

polarized epithelia, linear AJs associated with CAB are mainly formed at cell–cell junctions, thereby leading to formation of epithelial cell sheets covering the inner and outer surface of the body (Ayollo et al., 2009; Taguchi et al., 2011). In contrast, EC junctions are highly dynamic and morphologically heterogeneous, as ECs regulate the passage of solutes and nutrients between the blood and surrounding tissues (Millán et al., 2010; Hoelzle and Svitkina, 2012; Huveneers et al., 2012). In addition, the EC junctions need to be remodeled during processes such as leukocyte extravasation and sprouting angiogenesis (Dejana et al., 2008). Therefore, ECs establish both punctate AJs connected by RSF and linear AJs anchoring to CAB to regulate EC barrier function dynamically.

The balance between dynamic punctate AJs and stable linear AJs determines EC barrier function and is finely controlled by various extracellular stimuli. Inflammatory mediators including tumor necrosis factor-α, histamine, and thrombin induce formation of punctate AJs connected by RSF to increase EC permeability

Figure 1. **NM-II is required for Rap1-induced CAB formation.** (A) Monolayer-cultured HUVECs plated on collagen-coated dishes were stimulated with vehicle (Control) or 10 µM FSK for 20 min, immunostained with anti–VE-cadherin antibody, and stained with rhodamine-phalloidin (F-actin). VE-cadherin and F-actin images, the merged images (VE-cadherin, green; F-actin, red), and the bright field (BF) images are shown. (B) HUVECs were simulated with vehicle (Control), 10 µM FSK, 1 mM 8-pCPT-2′-O-methyl-cAMP (007), or 0.5 mM 6-Bnz for 20 min (the cells were stimulated with FSK, 007, and 6-Bnz at these concentrations for 20 min throughout the following experiments unless otherwise indicated), stained with rhodamine-phalloidin (F-actin), and immunostained

(Millán et al., 2010; Huveneers et al., 2012). In contrast, formation of linear AJs supported by CAB is induced by the factors that promote EC barrier function such as cAMP-elevating G protein–coupled receptor agonists, sphingosine-1-phosphate, and angiopoietin-1 (Garcia et al., 2001; Fukuhra et al., 2006; Augustin et al., 2009). We and others have previously reported that elevation of intracellular cAMP leads to CAB formation by activating a Rap1 small GTPase via exchange protein directly activated by cAMP (Epac), thereby inducing formation of linear AJs and stabilization of vascular endothelial cadherin (VE-cadherin)–based cell–cell junctions (Cullere et al., 2005; Fukuhara et al., 2005; Kooistra et al., 2005; Wittchen et al., 2005; Noda et al., 2010). Furthermore, VE-cadherin engagement results in Rap1 activation at nascent cell–cell contacts through PDZ-GEF, a guanine nucleotide exchange factor (GEF) for Rap1, which in turn facilitates maturation of AJs by inducing reorganization of the actin cytoskeleton (Sakurai et al., 2006; Pannekoek et al., 2011). Similarly, Rap1 is involved in the formation of E-cadherin–based cell–cell adhesions in epithelial cells (Hogan et al., 2004; Price et al., 2004). However, the mechanism underlying Rap1-induced CAB formation remains unknown.

Non-muscle myosin II (NM-II)–generated cytoskeletal tension is thought to be required for proper formation of AJs (Vicente-Manzanares et al., 2009; Gomez et al., 2011; Ratheesh and Yap, 2012). In epithelial cells, activation of NM-IIA by the Rho-Rho–associated coiled-coil containing protein kinase (ROCK) pathway regulates linear AJ formation by localizing E-cadherin at cell–cell contacts, whereas NM-IIB is known to localize at cell–cell junctions in a Rap1-dependent manner and regulate the CAB formation (Smutny et al., 2010). CAB formation produces the tension parallel to the cell–cell junctions. However, in ECs, the Rho–ROCK–NM-II pathway induces punctate AJ formation during remodeling of EC junctions (Millán et al., 2010; Hoelzle and Svitkina, 2012; Huveneers et al., 2012). In addition, inflammatory mediators activate the Rho–ROCK–NM-II pathway, which leads to EC contraction and barrier disruption, presumably by producing tension toward the center of the cell (Millán et al., 2010; Huveneers et al., 2012). However, the role of NM-II in Rap1-induced CAB formation in ECs remains unknown.

Here, we report that myotonic dystrophy kinase–related CDC42-binding kinase (MRCK; also known as CDC42BP)-mediated local activation of NM-II at cell–cell junctions is responsible for Rap1-induced CAB formation. Our present data suggest that Rap1 induces Cdc42 activation at cell–cell junctions, which leads to junctional activation of NM-II through MRCK, thereby promoting CAB formation. In addition, we found that Rap1 inhibits formation of RSF connecting to punctate AJs by suppressing the Rho–ROCK–NM-II pathway. Thus, we propose that Rap1 shifts the balance between two types of AJs—dynamic punctate AJs and stable linear AJs—by differentially regulating the Cdc42–MRCK–NM-II pathway and the Rho–ROCK–NM-II pathway.

Results

NM-II is required for CAB formation induced by Rap1

Stimulation with forskolin (FSK), an activator of adenylyl cyclase, led to disruption of RSF connecting to punctate AJs and formation of CAB supporting linear AJs (Figs. 1 A and S1 A). We have previously revealed that Rap1 mediates these FSK-induced responses (Fukuhara et al., 2005; Noda et al., 2010). To clarify the role of NM-II in Rap1-induced CAB formation, we investigated the effect of Rap1 activation on the NM-II activity by examining the localization of its regulatory light chain (RLC) phosphorylated at Ser19. In human umbilical vein ECs (HUVECs), phosphorylated RLC (pRLC) localized in the RSF, but was not observed at cell–cell contacts, under confluent culture condition (Fig. 1 B). Stimulation with FSK or 007, a cAMP analogue specific for Epac, induced RSF disruption, CAB formation, and RLC phosphorylation at cell–cell contacts (Fig. 1 B). In contrast, treatment with N^6-benzoyl-cAMP (6-Bnz), a cAMP analogue specific for PKA, affected neither organization of the actin cytoskeleton nor localization of pRLC (Fig. 1 B). Together with the evidence that FSK and 007, but not 6-Bnz, induced Rap1 activation (Fig. S1, B–D), these findings imply that FSK and 007 regulate the NM-II activity through Rap1. Consistently, either FSK- or 007-induced RSF disruption, CAB formation, and RLC phosphorylation at cell–cell contacts were prevented by depletion of Rap1 (Figs. 1 C and S1, E–G). These results indicate that Rap1 induces RSF disruption and CAB formation, and suggest that the latter might be caused by the NM-II activation at cell–cell contacts.

To investigate the requirement of NM-II for Rap1-induced CAB formation, we knocked down two isoforms of NM-II—NM-IIA and NM-IIB—because their role in AJ formation has been reported in epithelial cells (Smutny et al., 2010). FSK failed to induce CAB formation in the HUVECs depleted of NM-IIA and NM-IIB using siRNAs targeting NM-IIA and NM-IIB (Figs. 1 D and S1 H). In addition, knockdown of NM-IIA and NM-IIB prevented RSF formation in the unstimulated cells (Fig. 1 D). Consistently, inhibition of NM-II by blebbistatin, an inhibitor for myosin II, caused disruption of RSF in unstimulated cells and decreased CAB formation by FSK and 007 (Fig. 1, E and F). NM-II–generated tension is required for maintenance of linear AJ

with anti-pRLC (phosphorylated regulatory myosin light chain) at Ser19 (pRLC (Ser19)) and anti–VE-cadherin antibodies. F-actin, pRLC (Ser19), VE-cadherin images, and the merged images are shown. (C) HUVECs transfected with control siRNA or Rap1 siRNA #1 were stimulated with vehicle (Control), FSK, or 007, and stained similar to as in B. (D) HUVECs transfected with siRNA indicated at the left (control or two independent mixtures, #1 and #2, of NM-IIA and NM-IIB) were stimulated with vehicle (Control) or FSK, and stained with rhodamine-phalloidin. (E) HUVECs were pretreated with or without 20 µM blebbistatin for 4 h, stimulated with vehicle, FSK, or 007, and stained similar to as in A. (F) The F-actin that accumulated at cell–cell contacts, as observed in E, was quantified. Values are expressed as a percentage relative to that in the blebbistatin-untreated cells stimulated with vehicle, and shown as mean ± SEM (error bars) from three independent experiments ($n \geq 80$). **, P < 0.01, significant difference between two groups. In A and C–E, the boxed areas are enlarged in the insets (A, C, and E), or below the original images (D). Arrowheads (B–D) and parentheses (B) indicate cell–cell junctions and stress fibers, respectively. Bars, 10 µm.
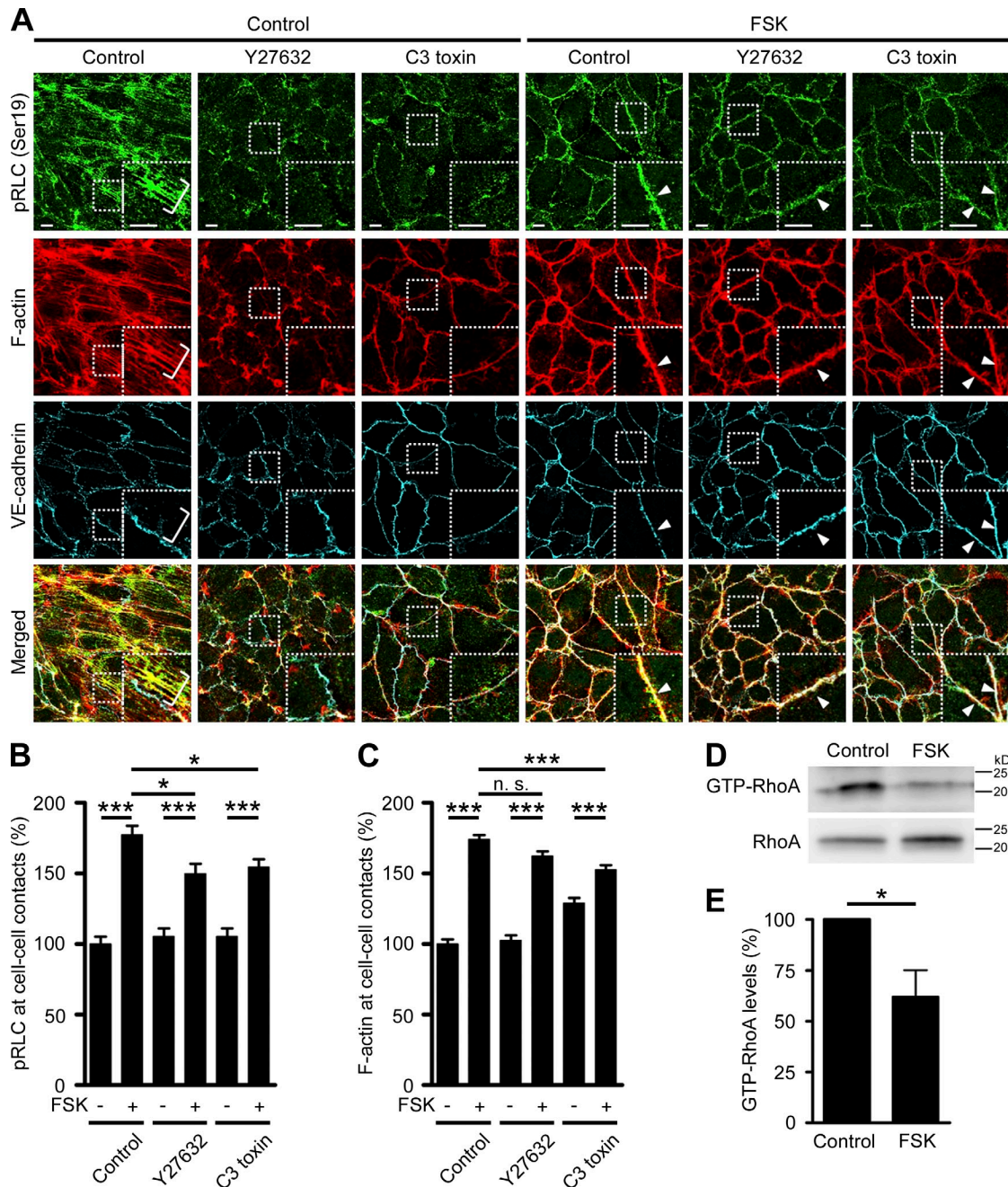
Figure 2. **The Rho–ROCK–NM-II pathway is required for RSF formation, but not for CAB formation.** (A) Monolayer-cultured HUVECs were treated without (Control) or with either 10 µg/ml C3 toxin for 24 h or 50 µM Y27632 for 30 min, stimulated with vehicle (Control) or FSK, and stained similar to as in Fig. 1 B. The boxed areas are enlarged in the insets. Arrowheads and brackets indicate cell–cell junctions and stress fibers, respectively. Bars, 10 µm. (B and C) Quantitative relative expression values of pRLC at Ser19 (B) and F-actin (C) at cell–cell contacts compared to those in the control cells without FSK stimulation observed in A are shown as mean ± SEM from three independent experiments (error bars; $n \geq 209$). (D and E) GTP-bound form of RhoA (GTP-RhoA) and total RhoA (RhoA) in the HUVECs stimulated with vehicle (Control) or FSK for 30 min were analyzed. In E, values are expressed as a percentage relative to that in control cells, and shown as mean ± SEM (error bars; $n \geq 7$). *, $P < 0.05$; ***, $P < 0.001$, significant difference between two groups. n.s., no significance between two groups.

structure (Vicente-Manzanares et al., 2009; Gomez et al., 2011; Ratheesh and Yap, 2012). Indeed, stimulation with FSK or 007 increased the linearity of cell–cell junctions, which was blocked by inhibition of NM-II (Fig. S1 I). Collectively, these findings indicate that Rap1 evokes NM-II activation at cell–cell contacts to induce formation of CAB supporting linear AJs, and also reveal the requirement of NM-II for formation of RSF connecting to punctate AJs in unstimulated ECs.

NM-II activation by the Rho–ROCK pathway is responsible for RSF formation, but not for Rap1-induced CAB formation

Next, we explored the mechanism by which Rap1 induces the NM-II activation required for CAB formation. ROCK, a downstream effector of Rho, is known to phosphorylate RLC of NM-II and regulate AJ formation in both epithelial cells and ECs (Abraham et al., 2009; Millán et al., 2010; Smutny et al., 2010;

Huveneers et al., 2012). Hence, we investigated whether the Rho–ROCK pathway is required for Rap1-induced activation of NM-II at cell–cell junctions. Either a Rho inhibitor C3 exoenzyme or a ROCK inhibitor Y27632 induced RSF disruption in unstimulated HUVECs (Fig. 2 A). In clear contrast, FSK-induced CAB formation and RLC phosphorylation at cell–cell junctions were only slightly inhibited by the treatment with C3 or Y27632 (Fig. 2, A–C). Furthermore, FSK-increased junctional linearity was not inhibited by treatment with C3 toxin (Fig. S1 J). These results reveal that Rho–ROCK pathway–mediated activation of NM-II is required for RSF formation, but is dispensable for Rap1-induced CAB formation.

Because RSF was inhibited either by inhibition of the Rho–ROCK–NM-II pathway or by activation of Rap1, we hypothesized that Rap1 might induce RSF disruption through inhibition of the Rho–ROCK–NM-II pathway. RhoA activity was suppressed by stimulation with either FSK or 007 (Fig. 2, D and E; and Fig. S2, A and B). These observations suggest that Rap1 spatially controls the NM-II activity by inhibiting ROCK and by activating kinases other than ROCK that phosphorylate RLC of NM-II at cell–cell junctions, thereby inducing RSF disruption and CAB formation.

MRCK is involved in Rap1-induced NM-II activation leading to CAB formation

We sought to identify the kinases that act downstream of Rap1 to induce RLC phosphorylation in ECs. The kinases that induce phosphorylation of RLC of NM-II can be divided into two groups (Ikebe and Hartshorne, 1985; Chew et al., 1998; Leung et al., 1998; Yamashiro et al., 2003; Yoneda et al., 2005; Tan et al., 2011); one group includes the kinases that induce monophosphorylation of RLC at Ser19 and the other contains those that evoke di-phosphorylation of RLC at Thr18/Ser19. Hence, we examined whether Rap1 induces monophosphorylation or diphosphorylation of RLC of NM-II. In unstimulated ECs, both monophosphorylated and diphosphorylated RLC localized in the RSF (Figs. 3 A and S2 C). In contrast, monophosphorylated, but not diphosphorylated, RLC of NM-II localized on the CAB in FSK- or 007-stimulated cells (Figs. 3 A and S2 C), which suggests that Rap1 induces NM-II activation through the kinase that induces monophosphorylation of RLC.

Among the kinases involved in activation of NM-II, MRCK and p21-activated kinases (PAK) induce monophosphorylation of the RLC at Ser19 (Chew et al., 1998; Leung et al., 1998; Tan et al., 2011). PAK has been shown to increase EC permeability through NM-II–mediated EC contraction or by phosphorylating VE-cadherin (Zeng et al., 2000; Stockton et al., 2004; Gavard and Gutkind, 2006). PAK also induces dephosphorylation of RLC by inhibiting myosin light chain kinase (Sanders et al., 1999; Wirth et al., 2003). Therefore, we decided to study the role of MRCK in Rap1-induced NM-II activation and CAB formation, as its function in ECs has never been investigated.

RT-PCR analysis revealed the expression of two isoforms of MRCK—MRCKα and MRCKβ—in ECs (Fig. S2 D). Knockdown of both isoforms did not affect RSF formation in unstimulated HUVECs, but clearly inhibited FSK- or 007-induced CAB

formation and monophosphorylation of RLC at cell–cell contacts, although these effects were partially inhibited by depletion of either isoform (Figs. 3, B–E; and Fig. S2, E–I). Consistently, depletion of MRCKα and MRCKβ, although not statistically significant, marginally reduced monophosphorylation of RLC in FSK-stimulated HUVECs but not in the unstimulated cells (Fig. S2, J and K). In contrast, diphosphorylation of RLC was unaffected by the depletion of both isoforms (Fig. S2, J and K). In addition, inhibition of FSK-induced CAB formation and monophosphorylation of RLC at cell–cell junctions by depletion of MRCKα and MRCKβ was rescued by expression of MRCKβ tagged with GFP (MRCKβ-GFP) encoded by an siRNA-insensitive construct (Fig. 3, F–H). Moreover, FSK induced association of MRCK with NM-II (Fig. S2 M). These findings indicate that MRCK acts downstream of Rap1 to induce NM-II activation and CAB formation, but is dispensable for RSF formation.

MRCK is recruited to cell–cell junctions by Rap1 in a Cdc42-dependent manner

To address the mechanism by which MRCK mediates Rap1-induced activation of NM-II at cell–cell junctions, we investigated the localization of MRCK by expressing the MRCKβ-GFP in HUVECs. MRCKβ-GFP localized in the cytoplasm of unstimulated cells, whereas it was recruited to cell–cell junctions upon stimulation with FSK or 007 (Figs. 4 A, S3 A, and S4 B). Although GFP signal was observed at cell–cell contacts in GFP-expressing cells, it was not dependent on the junctional localization of GFP, but ascribed to the overlap of plasma membrane (Fig. S3 A). FSK failed to induce translocation of MRCKβ-GFP to cell–cell junctions in the cells depleted of Rap1 (Fig. 4 B), which indicates that MRCK recruitment to cell–cell junctions needs Rap1.

We further tried to identify the signaling molecule that mediates Rap1-induced localization of MRCK at cell–cell contacts. MRCK is known to be a Cdc42 effector. Indeed, MRCKβ-GFP bound to the activated form of Cdc42, but not those of Rac1 and RhoA (Fig. 4 C). In addition, Cdc42 is known to promote EC barrier function (Broman et al., 2007; Ramchandran et al., 2008). Therefore, we investigated the role of Cdc42 in Rap1-induced localization of MRCK at cell–cell junctions. FSK-induced recruitment of MRCKβ-GFP to cell–cell junctions was inhibited by depletion of Cdc42 (Fig. 4 D). Furthermore, a MRCKβ mutant (MRCKβ H1593/1596A-GFP) that is incapable of binding to the active form of Cdc42 failed to localize at cell–cell junctions even upon stimulation with 007 (Fig. 4, C and E). These results indicate that Rap1 induces recruitment of MRCK to cell–cell junctions through Cdc42.

Rap1 induces accumulation of active Cdc42 at cell–cell junctions to regulate localization of MRCK

The next question is how Cdc42 mediates Rap1-induced localization of MRCK at cell–cell junctions. Because the MRCK mutant lacking the Cdc42 binding site could not localize at cell–cell contacts (Fig. 4 E), we hypothesized that Rap1 increases the active Cdc42 at cell–cell contacts. To address this, we examined the localization of active Cdc42 by visualizing the GFP-tagged Cdc42/Rac interactive binding domain of neural Wiskott Aldrich syndrome

Figure 3. MRCK is required for Rap1-induced NM-II activation leading to CAB formation. (A) HUVECs were stimulated with vehicle (Control) or FSK, immunostained with the antibodies indicated in the top panels, and stained with rhodamine-phalloidin (F-actin). pRLC (Ser19) or ppRLC (Thr18/Ser19) images, F-actin images, and the merged images (pRLC (Ser19) or ppRLC (Thr18/Ser19), green; F-actin, red) are shown. (B) Lysates from the HUVECs transfected without (No siRNA) or with control siRNA or MRCK siRNA targeting both MRCKα and MRCKβ for 2 d were subjected to Western blot analyses with anti-MRCKα, anti-MRCKβ, and anti–β-actin antibodies. (C) HUVECs transfected with control or MRCK siRNA were stimulated with vehicle (Control) or FSK, and stained similar to as in Fig. 1 B. (D and E) Quantitative relative expression values of pRLC at Ser19 (D) and F-actin (E) at cell–cell contacts compared to those in control siRNA-transfected cells without FSK stimulation observed in C were expressed as mean ± SEM (error bars; $n \geq 40$). Similar results were obtained in three independent experiments. (F) HUVECs expressing either GFP or siRNA-insensitive MRCKβ-GFP were transfected with control or MRCK siRNA, stimulated with FSK, immunostained with anti-pRLC at Ser19 (pRLC (Ser19)) antibody, and stained with rhodamine-phalloidin (F-actin). pRLC (Ser19), F-actin, and GFP images are shown. Note that GFP signal at cell–cell contacts between the cells expressing GFP is ascribed to the overlap of plasma membrane (see Fig. S3 A). (G and H) Quantitative relative expression values of pRLC at Ser19 (G) and F-actin (H) at cell–cell contacts compared to those in GFP-expressing and control siRNA-transfected cells without FSK stimulation observed in F are given as mean ± SEM (error bars; $n \geq 40$). Similar results were obtained in three independent experiments. In A, C, and F, the boxed areas are enlarged in the insets. Arrowheads (A, C, and F) and brackets (C) indicate cell–cell junctions and stress fibers, respectively. *, $P < 0.05$; **, $P < 0.01$; ***, $P < 0.001$, significant difference between two groups. n.s., no significance between two groups. Bars, 10 µm.
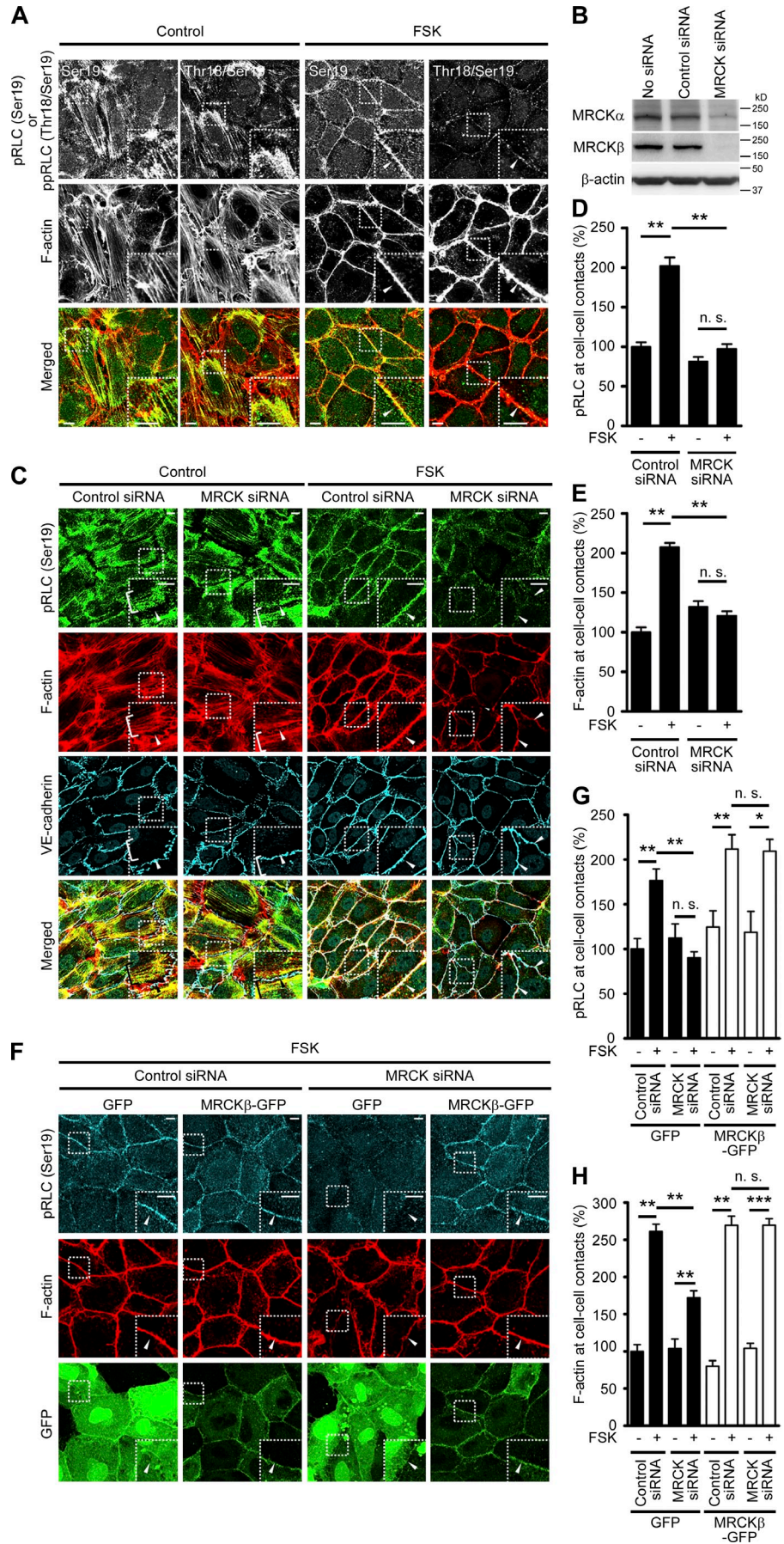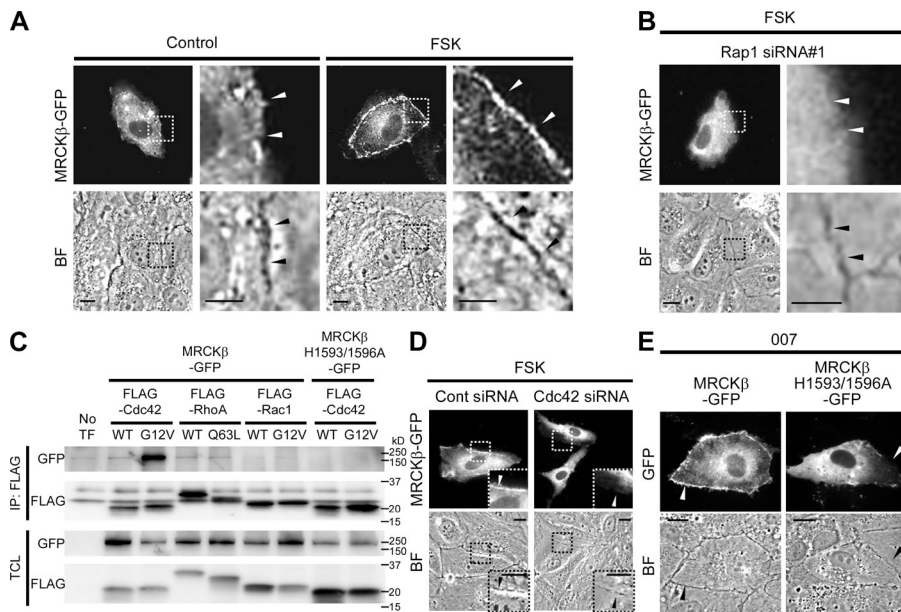
Figure 4. **Rap1-dependent translocation of MRCK to cell–cell junctions is mediated by Cdc42.** (A) HUVECs transfected with the plasmid encoding MRCKβ-GFP were stimulated with vehicle (Control) or FSK. GFP (MRCKβ-GFP) and bright field (BF) images are shown. The boxed areas are enlarged in the panels to the right of the original images. (B) HUVECs transfected with the plasmid encoding MRCKβ-GFP together with Rap1 siRNA #1 were stimulated with FSK similar to as in A. (C) 293T cells were transfected with the plasmid encoding either MRCKβ-GFP or MRCKβ H1593/1596A-GFP together with the vector expressing either FLAG-tagged wild type or constitutive active mutant of Cdc42 (Cdc42 WT and Cdc42 G12V), RhoA (RhoA WT and RhoA Q63L), and Rac1 (Rac1 WT and Rac1 G12V), as indicated at the top. Immunoprecipitates (IP: FLAG) of cell lysates and aliquots of total cell lysates (TCL) were subjected to Western blot analyses with anti-GFP and anti-FLAG antibodies as indicated on the left. (D) HUVECs transfected with either control siRNA or Cdc42 siRNA for 48 h were subsequently transfected with the vector encoding MRCKβ-GFP for 24 h, and stimulated with FSK similar to as in A. The boxed areas are enlarged in the insets. (E) HUVECs transfected with the plasmid encoding either MRCKβ-GFP or MRCKβ H1593/1596A-GFP were stimulated with 007 similar to as in A. Arrowheads indicate cell–cell junctions. Bars: (low magnification images in A and B, D, and E) 10 µm; (high magnification images in A and B) 5 µm.

protein (GFP-N-WASP), which specifically binds to active Cdc42 (Fig. S3 B). GFP-N-WASP was found in the cytoplasm of unstimulated HUVECs (Fig. 5 A). However, GFP-N-WASP, but not its mutant lacking the Cdc42 binding site (GFP-N-WASP H211D), was recruited to cell–cell junctions upon stimulation with either FSK or 007 (Figs. 5 A and S3, C and D). 007-induced localization of GFP-N-WASP at cell–cell contacts was blocked by depletion of Rap1 (Fig. 5 A). These findings suggest that Rap1 induces accumulation of active Cdc42 at cell–cell contacts.

To explore the mechanism of Rap1-induced accumulation of active Cdc42 at cell–cell junctions, we investigated the effect of Rap1 signaling on localization and activation of Cdc42 in ECs. Immunostaining of Cdc42-depleted HUVECs revealed that Cdc42 is recruited to the cell–cell contacts by stimulation with FSK or 007 (Figs. 5 B and S3 E). It should also be noted that VE-cadherin organization was compromised in Cdc42-depleted cells (Fig. 5 B), which suggests the crucial role of Cdc42 in EC junctions. Exogenously expressed FLAG-tagged Cdc42 also accumulated at cell–cell contacts upon stimulation with FSK (Fig. 5 C). In addition, Cdc42 colocalized with MRCK at cell–cell junctions in FSK-stimulated HUVECs (Fig. 5 D). By visualizing the Cdc42 activation using a FRET-based biosensor for Cdc42, we found that stimulation with either FSK or 007 induced Cdc42 activation in the marginal region of HUVECs that includes the cell–cell junctions (Fig. 5, E and F). These findings reveal that Rap1 increases the active Cdc42 at cell–cell contacts by inducing localization and activation of Cdc42 at cell–cell junctions, thereby leading to the recruitment of MRCK to the cell–cell junctions.

Cdc42 mediates Rap1-induced NM-II activation and CAB formation at cell–cell contacts through MRCK

We investigated whether Cdc42-mediated translocation of MRCK to cell–cell junctions is responsible for Rap1-induced

NM-II activation and CAB formation at cell–cell contacts. FSK and 007 failed to induce RLC phosphorylation and CAB formation at cell–cell contacts in the Cdc42-depleted HUVECs, although RSF formation was unaffected by knockdown of Cdc42 in unstimulated cells (Figs. 6 A and S3, F and G). However, FSK and 007 caused RSF disruption even in Cdc42-depleted cells, implying that Rap1 inhibits Rho-dependent RSF formation independently of Cdc42 (Figs. 6 A and S3 G). Inhibition of FSK-induced CAB formation by depletion of Cdc42 was cancelled by expression of Cdc42 encoded by an siRNA-insensitive plasmid (Fig. S3 H). Consistently, overexpression of a dominant-negative mutant of Cdc42 led to the inhibition of FSK-induced CAB formation (Fig. S3 I). Furthermore, the inhibition of FSK-induced CAB formation and RLC phosphorylation at cell–cell contacts by knockdown of MRCK was reversed by expression of MRCKβ-GFP, but not by that of MRCKβ H1593/1596A-GFP (Fig. 6, B–D). Unexpectedly, FSK-induced CAB formation and RLC phosphorylation at cell–cell contacts was inhibited by overexpression of MRCKβ H1593/1596A-GFP (Fig. 6, B–D). Because MRCKα forms a multimer (Tan et al., 2001), this protein may act as a dominant-negative mutant by associating with and inhibiting endogenous MRCK. Collectively, these results indicate that Rap1 induces NM-II activation at cell–cell contacts through Cdc42-mediated recruitment of MRCK to cell–cell junctions, thereby promoting CAB formation.

FGD5 acts downstream of Rap1 to induce Cdc42 activation at cell–cell contacts

How does Rap1 induce accumulation of active Cdc42 at cell–cell contacts? It has been reported that FYVE, RhoGEF, and PH domain–containing protein 5, also known as facio-genital dysplasia-5 (FGD5), a GEF for Cdc42, is expressed in ECs and partially localizes at cell–cell junctions (Kurogane et al., 2012). Hence, we investigated the role of FGD5 in Rap1-induced activation of Cdc42 at cell–cell junctions. In unstimulated
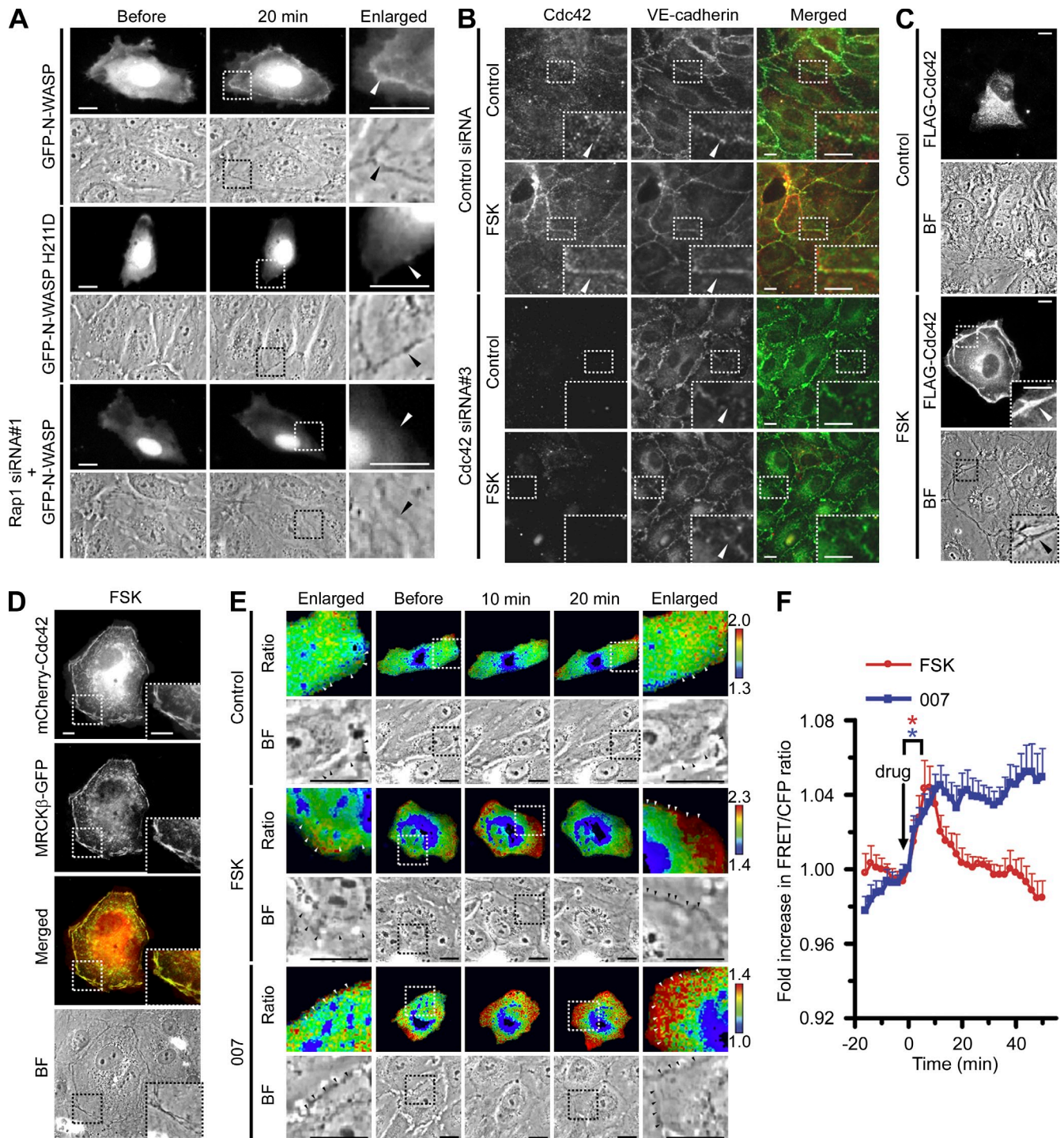
Figure 5. **Rap1 induces accumulation of active Cdc42 at cell–cell junctions.** (A) HUVECs transfected with the N-WASP–expressing plasmids indicated on the left, GFP-tagged CRIB domain of N-WASP (GFP-N-WASP), or the mutant lacking Cdc42 binding site (GFP-N-WASP H211D) were stimulated with 007. The cells transfected with the plasmid encoding GFP-N-WASP together with Rap1 siRNA #1 were also stimulated with 007 (bottom two rows). GFP and bright field (BF) images acquired before and 20 min after the stimulation are shown. (B) HUVECs transfected with either control siRNA or Cdc42 siRNA #3 were stimulated with vehicle (Control) or FSK and immunostained with anti-Cdc42 and anti–VE-cadherin antibodies. Images of Cdc42 and VE-cadherin and the merged images (Cdc42, red; VE-cadherin, green) are shown. (C) HUVECs transfected with the plasmid expressing FLAG-Cdc42 were stimulated with either vehicle (Control) or FSK and immunostained with anti-FLAG antibody. FLAG-Cdc42 and BF images are shown. (D) HUVECs cotransfected with the plasmid encoding mCherry-Cdc42 and that encoding MRCKβ-GFP were stimulated with FSK. mCherry (mCherry-Cdc42) and GFP (MRCKβ-GFP) images, the merged images (mCherry, red; GFP, green) and the BF images are shown. (E) HUVECs expressing RaichuEV-Cdc42, a FRET-based Cdc42 activity-monitoring probe, were stimulated with vehicle (Control), FSK, or 007 and subjected to time-lapse FRET imaging. The images were obtained every 2 min for 16 min before and 50 min after the stimulation. Representative ratio images of FRET/CFP at the indicated time points are shown in the intensity-modulated display mode (IMD). The upper and lower limits of the ratio image with IMD are indicated on the right. The boxed areas in the images acquired before and after the stimulation are enlarged on the left and right sides of the original images, respectively. (F) The fold increase of the FRET/CFP ratio observed in E was calculated by dividing the FRET/CFP ratio in the cells stimulated with either FSK (red line) or 007 (blue line) by those in the vehicle-treated cells at the
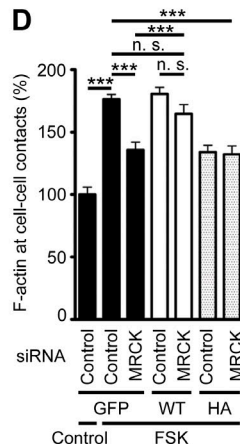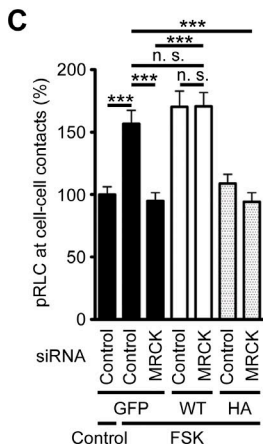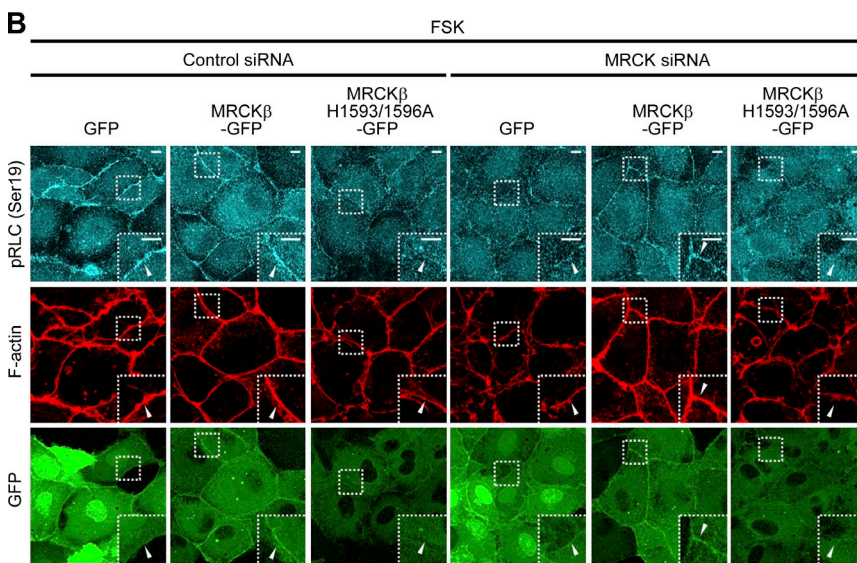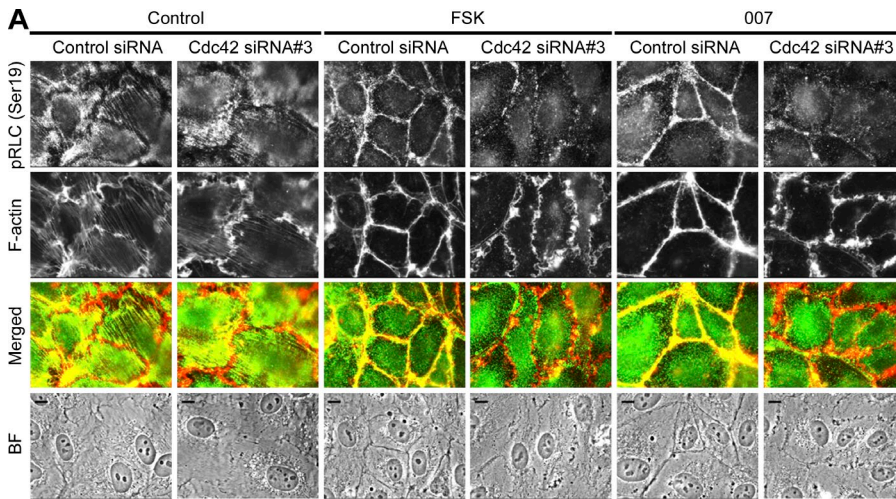
Figure 6. Cdc42 is required for Rap1-induced activation of NM-II and formation of CAB at cell–cell junctions. (A) HUVECs transfected with either control siRNA or Cdc42 siRNA #3 were stimulated with vehicle (Control), FSK, or 007, immunostained with anti-pRLC at Ser19 (pRLC (Ser19)) antibody, and stained with rhodamine-phalloidin (F-actin). pRLC (Ser19) and F-actin images, the merged images (F-actin, red; pRLC (Ser19), green), and the bright field images (BF) are shown. Bars, 10 µm. (B) HUVECs expressing GFP, siRNA-insensitive MRCKβ-GFP, or siRNA-insensitive MRCKβ H1593/1596A-GFP were transfected with either control siRNA or MRCK siRNA, stimulated with FSK, and stained similar to as in Fig. 3 F. Arrowheads indicate cell–cell junctions. Bars, 10 µm. (C and D) Quantitative relative values of pRLC at Ser19 (C) and F-actin (D) at cell–cell contacts in the cells expressing GFP, MRCKβ-GFP (WT), or MRCKβ H1593/1596A-GFP (HA) compared to those in GFP-expressing and control siRNA-transfected cells without FSK stimulation observed in B are shown as mean ± SEM (error bars; n ≥ 40). Similar results were obtained in three independent experiments. ***, P < 0.01, significant difference between two groups. n.s., no significance between two groups.

corresponding time points. The drugs were added to the culture media at time 0 as indicated by the arrow. Data are expressed as fold increase relative to that at time 0, and shown as mean ± SEM (error bars) of seven independent experiments. Significant differences between the value at 0 min and that at 8 min after the stimulation are indicated as *, P < 0.05. The boxed areas are enlarged on the right side of the original images (A) or in the insets (B–D). Arrowheads indicate cell–cell junctions. Bars, 10 µm.
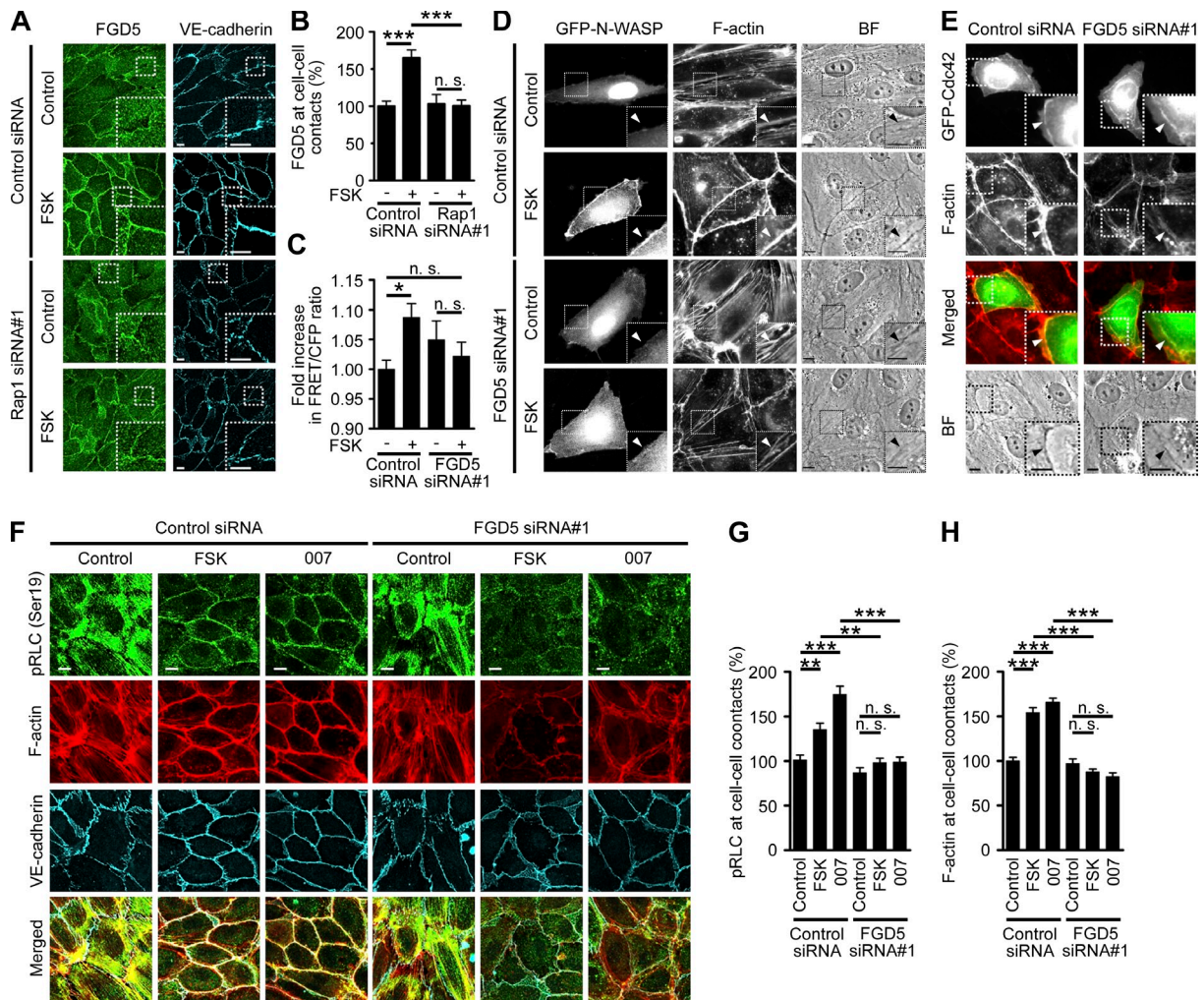
Figure 7. **FGD5 is required for Rap1-induced CAB formation via activation of Cdc42 at cell–cell junctions.** (A) HUVECs transfected with control siRNA or Rap1 siRNA #1 were stimulated with vehicle (Control) or FSK, and immunostained with anti-FGD5 and anti–VE-cadherin antibodies. (B) Quantitative relative expression values of FGD5 at cell–cell contacts compared to those in control siRNA-transfected cells stimulated with vehicle observed in A are shown as mean ± SEM (error bars) from three independent experiments ($n \geq 80$). (C) RaichuEV-Cdc42–expressing HUVECs transfected with control siRNA or FGD5 siRNA #1 were stimulated with vehicle (Control) or FSK, and subjected to time-lapse FRET imaging similar to as in Fig. 5 E. The fold increase in FRET/CFP ratios 10 min after the stimulation were calculated similar to as in Fig. 5 F and shown as mean ± SEM (error bars) from four independent experiments ($n \geq 36$). (D) HUVECs transfected with either control siRNA or FGD5 siRNA #1 for 48 h were subsequently transfected with the plasmid encoding GFP-N-WASP for 24 h, stimulated with vehicle (Control) or FSK, and stained with rhodamine-phalloidin (F-actin). GFP (GFP-N-WASP), F-actin, and bright field (BF) images are shown. (E) HUVECs transfected with the plasmid encoding GFP-Cdc42 together with either control siRNA or FGD5 siRNA #1 were stimulated with FSK, and stained with rhodamine-phalloidin. GFP and F-actin images, the merged images (GFP, green; F-actin, red), and BF images are shown. (F) HUVECs transfected with either control siRNA or FGD5 siRNA #1 were stimulated similar to as in Fig. 1 B. (G and H) Quantitative relative expression values of pRLC at Ser19 (G) and F-actin (H) at cell–cell contacts compared to those in control siRNA-transfected cells treated with vehicle in F are shown as mean ± SEM (error bars; $n = 33$). Similar results were obtained in three independent experiments. In A, D, and E, the boxed areas are enlarged in the insets. In D and E, arrowheads indicate cell–cell junctions. *, $P < 0.05$; **, $P < 0.01$; ***, $P < 0.001$, significant difference between two groups. n.s., no significance between two groups. Bars, 10 µm.

HUVECs, FGD5 localized at the plasma membrane and partially at cell–cell junctions, as previously reported (Kurogane et al., 2012; Fig. 7 A). Stimulation with FSK enhanced junctional localization of FGD5 (Fig. 7, A and B). However, FSK did not alter localization of FGD5 in the Rap1-depleted cells (Fig. 7, A and B), which suggests that FGD5 may mediate Rap1-induced Cdc42 activation at cell–cell junctions. Consistently, FGD5 depletion prevented not only FSK-induced Cdc42 activation but also FSK-induced accumulation of active Cdc42 at cell–cell junctions (Fig. 7, C and D; and Fig. S4 A). However, FSK-induced recruitment of Cdc42 to cell–cell contacts occurred even in the absence of FGD5 expression (Fig. 7 E). In addition,

007-induced junctional localization of MRCKβ-GFP was abrogated by depletion of FDG5 (Fig. S4 B). Consistently, FSK-or 007-induced RLC phosphorylation and CAB formation at cell–cell junctions were inhibited by depletion of FGD5 (Fig. 7, F–H; and Fig. S4, C–E). The effect of FGD5 knockdown was cancelled by expression of FGD5 encoded by a plasmid expressing siRNA-insensitive mRNA for FGD5 (Fig. S4 F). These results suggest that Rap1 induces accumulation of active Cdc42 at cell–cell junctions through FGD5-independent localization of Cdc42 and FGD5-dependent activation of Cdc42 at cell–cell junctions, thereby promoting CAB formation by locally activating the MRCK–NM-II pathway.
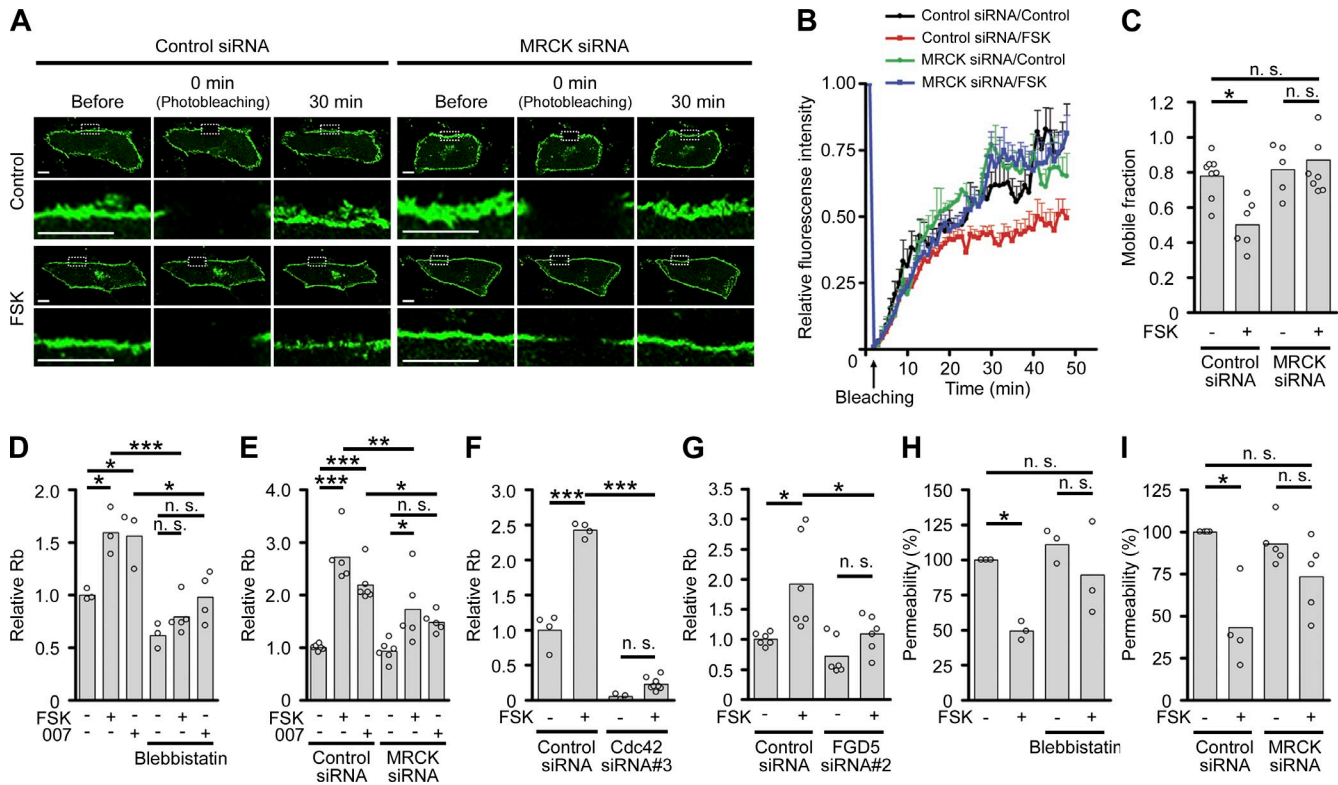
Figure 8. **The FGD5–Cdc42–MRCK–NM-II pathway is essential for Rap1-induced potentiation of EC barrier function.** (A) VE-cadherin–GFP-expressing HUVECs transfected with control or MRCK siRNA were stimulated with vehicle (Control) or FSK and subjected to FRAP analysis. Representative GFP images before and at the indicated time points after photobleaching (at 0 min) are shown. The photobleached regions are boxed and enlarged beneath the original images. Bars: (top panels) 10 µm; (bottom panels) 5 µm. (B) Quantitative analysis of FRAP experiments in A. A plot of relative fluorescence intensity of VE-cadherin-GFP compared to that of pre-photobleaching in control siRNA-transfected cells stimulated with vehicle (black) or FSK (red) or in MRCK siRNA-transfected cells stimulated with vehicle (green) or FSK (blue) is shown as mean ± SEM (error bars; $n \geq 5$). (C) The mobile fractions of VE-cadherin-GFP calculated from the fluorescence recovery curves observed in B are shown. Bars and circles indicate averages and individual data points, respectively ($n \geq 5$). (D–G) The junctional resistance between the adjacent cells (Rb) was measured using the ESIC system as described in the Materials and methods section. Relative Rb values to the matched control at 30 min after the stimulation are shown. Bars and circles indicate averages and individual data points, respectively ($n \geq 3$). In D, confluent HUVECs cultured for overnight were stimulated with vehicle, FSK, or 007 in the absence or presence of blebbistatin. The control value is that in blebbistatin-untreated cells stimulated with vehicle. In E, F, and G, HUVECs transfected with control siRNA or MRCK (E), Cdc42 #3 (F), or FGD5 #2 siRNA (G) were stimulated with vehicle, FSK, or 007. The control values are those in the control siRNA-transfected cells stimulated with vehicle. (H) EC permeability in the monolayer-cultured HUVECs stimulated with vehicle or FSK in the absence or presence of blebbistatin was analyzed. Relative permeability of each group of the cells compared with that in blebbistatin-untreated cells stimulated with vehicle is shown. (I) EC permeability in control siRNA– or MRCK siRNA–transfected HUVECs stimulated with vehicle or FSK was analyzed. Relative permeability of each group of the cells compared with that in control siRNA-transfected cells stimulated with vehicle is shown. In H and I, bars and circles indicate averages and individual data points, respectively ($n \geq 3$). *, P < 0.05; **, P < 0.01; ***, P < 0.001, significant difference between two groups. n.s., no significance between two groups.

Rap1 potentiates EC barrier function by inducing CAB formation through the signaling pathway involving FGD5, Cdc42, MRCK, and NM-II

We have previously reported that Rap1 enhances stabilization of VE-cadherin–dependent cell adhesion by inducing CAB formation (Noda et al., 2010). Therefore, we tested whether MRCK is required for Rap1-induced stabilization of VE-cadherin–dependent cell adhesion by performing FRAP analysis using VE-cadherin tagged with GFP (VE-cadherin-GFP). The mobile fraction of VE-cadherin-GFP at cell–cell contacts was significantly reduced by stimulation with FSK (Fig. 8, A–C). However, this effect was completely abolished by knockdown of MRCK (Fig. 8, A–C). These findings suggest that Rap1 stabilizes VE-cadherin–dependent cell adhesion through MRCK-mediated CAB formation.

Finally, we investigated the functional significance of the signaling pathway involving FGD5, Cdc42, MRCK, and NM-II

in Rap1-induced potentiation of EC barrier function. To this end, we used the electric cell-substrate impedance sensing (ECIS) technique, which allows us to evaluate barrier function by measuring the junctional resistance between the adjacent cells (Rb). In confluent HUVECs, the Rb was significantly elevated by stimulation with FSK and 007 (Figs. 8 D and S5, A–C). However, FSK and 007 failed to increase the Rb either in the cells depleted of Rap1 or in the presence of latrunculin A, an actin polymerization inhibitor, which prevented FSK-induced CAB formation (Fig. S5, A–H). These findings indicate that Rap1 potentiates EC barrier functions by inducing CAB formation. In addition, inhibition of NM-II by blebbistatin or depletion of MRCK, Cdc42, or FGD5 significantly inhibited the Rb elevation induced by FSK and 007 (Figs. 8, D–G; and S5, I–M). Consistently, permeability of EC monolayers was decreased by stimulation with FSK, as assessed by in vitro vascular permeability assay (Fig. 8, H and I). However, FSK did not reduce EC permeability either in the presence of blebbistatin or in the cells depleted

of MRCK (Fig. 8, H and I). Collectively, these results suggest that Rap1 potentiates EC junctions by inducing CAB formation through the FGD5–Cdc42–MRCK–NM-II signaling axis.

Discussion

Rap1 potentiates EC junctions by inducing formation of CAB that stabilizes linear AJs. Here, we demonstrate that the Cdc42–MRCK pathway–mediated junctional activation of NM-II is essential for Rap1-induced CAB formation. Activation of Rap1 caused accumulation of active Cdc42 at cell–cell contacts, which locally stimulated the NM-II activity by recruiting MRCK to cell–cell junctions, thereby enhancing EC barrier function. Although several lines of evidence suggest the role of MRCK in cell migration (Gomes et al., 2005; Wilkinson et al., 2005; Gaggioli et al., 2007; Tan et al., 2008), its function in formation of EC junctions has not been investigated. Thus, this study uncovers a novel role for MRCK in Rap1-induced formation of AJs in ECs.

Our present data suggest that the FGD5–Cdc42–MRCK–NM-II signaling pathway acts downstream of Rap1 to induce CAB formation and EC barrier function. However, it has not been proven whether these signaling molecules act in a linear pathway. Thus, further study is required to determine the signaling hierarchy downstream of Rap1 to promote CAB formation and EC barrier function.

Rap1 potentiates EC junctions not only by stimulating the Cdc42–MRCK–NM-II pathway but also by suppressing the Rho–ROCK–NM-II pathway. During remodeling of EC junctions, the Rho–ROCK–NM-II pathway induces formation of punctate AJs that connect to RSF through VE-cadherin/β-catenin/α-catenin complexes (Abraham et al., 2009; Millán et al., 2010; Hoelzle and Svitkina, 2012; Huveneers et al., 2012; Wimmer et al., 2012). The Rho–ROCK pathway also disrupts blood–brain barrier integrity through phosphorylation of occludin and claudin-5 (Yamamoto et al., 2008). In addition, inflammatory mediators activate the Rho–ROCK–NM-II pathway to increase actomyosin-driven pulling forces generated on the punctate AJs, thereby leading to EC contraction and barrier disruption (Millán et al., 2010; Huveneers et al., 2012). However, Rap1 is known to counteract inflammatory mediator-evoked barrier disruption through suppression of Rho activity (Cullere et al., 2005). In this study, we showed that Rap1 induces linear AJ formation through junctional activation of the Cdc42–MRCK–NM-II pathway and blunts punctate AJ formation through suppression of the Rho–ROCK–NM-II pathway. Thus, Rap1 may potentiate EC junctions by inducing transformation of dynamic punctate AJs into stable linear AJs not only under resting conditions but also in the presence of barrier disrupting agents.

Krit-1 might be involved in Rap1-mediated potentiation of EC junctions. Krit-1 is a Rap1 effector involved in regulation of EC junctions (Glading et al., 2007). Mutation of *Krit-1* is associated with familial cerebral cavernous malformation and causes disruption of EC barrier function by sustaining high levels of Rho and ROCK activities (Borikova et al., 2010; Stockton et al., 2010). Therefore, Rap1 may inhibit formation of punctate AJs by suppressing the Rho–ROCK–NM-II pathway through Krit-1.

Rap1-mediated activation of the Cdc42–MRCK–NM-II pathway might be conserved in AJ formation in epithelial cells. Rap1 is involved in the formation of E-cadherin–based cell adhesion in epithelial cells (Knox and Brown, 2002; Hogan et al., 2004; Price et al., 2004). Furthermore, Smutny et al. (2010) have reported that NM-IIB localizes at cell–cell junctions in a Rap1-dependent manner to regulate formation of the apical F-actin ring. In addition, the role of Cdc42 in epithelial AJ formation has been reported. Tuba, a Cdc42-specific GEF, activates Cdc42 to regulate the junctional configuration of simple epithelial cells (Otani et al., 2006). Moreover, ligation of nectin, which is one of the AJ components, induces Rap1 activation responsible for Src-dependent activation of Cdc42 in epithelial cells (Fukuhara et al., 2004; Fukuyama et al., 2005). Therefore, Cdc42–MRCK–NM-II signaling might be involved in epithelial AJ formation.

In this study, FGD5 was identified as a downstream signaling molecule from Rap1 to induce Cdc42 activation at EC junctions. FGD5 expressed in ECs functions in vascular formation (Cheng et al., 2012; Kurogane et al., 2012; Nakhaei-Nejad et al., 2012). FGD1-related Cdc42 GEF, another member of FGD family, has also been suggested to regulate Rap1-induced activation of Cdc42 in epithelial cells (Fukuyama et al., 2005). Thus, some FDG family members may serve as a GEF for Cdc42 acting downstream of Rap1. However, the molecular mechanism how Rap1 induces Cdc42 activation through FGD5 still remains unclear. Activation of Rap1 led to accumulation of FGD5 at cell–cell contacts. Moreover, Rap1-induced activation of Cdc42 was prevented by FGD5 depletion, suggesting that Rap1 induces junctional activation of Cdc42 by localizing FGD5 at cell–cell contacts. However, Rap1 may regulate FGD5 localization indirectly, as our preliminary data suggested no direct binding of FGD5 with active Rap1. Thus, further study is needed to clarify the mechanism underlying Rap1-induced junctional localization of FGD5. In addition, Rap1 induced accumulation of active Cdc42 at cell–cell junctions not only through FGD5-dependent activation of Cdc42 but also by localizing Cdc42 at cell–cell junctions through an as yet unidentified mechanism. Therefore, further examination is also required to elucidate the mechanism for Rap1-induced junctional localization of Cdc42.

In conclusion, we demonstrate that Rap1 signal induces CAB formation by locally stimulating the Cdc42–MRCK–NM-II pathway at cell–cell junctions to establish linear AJs (Fig. 9). Simultaneously, Rap1 inhibits formation of punctate AJs connected by RSF through suppression of the Rho–ROCK–NM-II pathway. Thus, Rap1 potentiates EC junctions by spatially controlling the NM-II activity (Fig. 9).

Materials and methods

Materials and antibodies
Materials were purchased as follows: FSK and latrunculin A from EMD Millipore; 8-pCPT-2′-O-methyl-cAMP (referred to as 007) from Tocris Bioscience; 6-Bnz from Biolog Life Science Institute; (R)-(+)-trans-N-(4-pyridyl)-4-(1-aminoethyl)-cyclohexanecarboxamide 2HCl H$_2$O (Y27632) from Wako Pure Chemicals; (−)-blebbistatin from Sigma-Aldrich; exoenzyme C3 transferase (C3 toxin) from Cytoskeleton, Inc.; and Cellmatrix type I-C from Nitta Gelatin Inc. Antibodies used here were purchased as follows: mouse anti–VE-cadherin and anti-Cdc42 from BD; anti-Rap1 from Santa Cruz
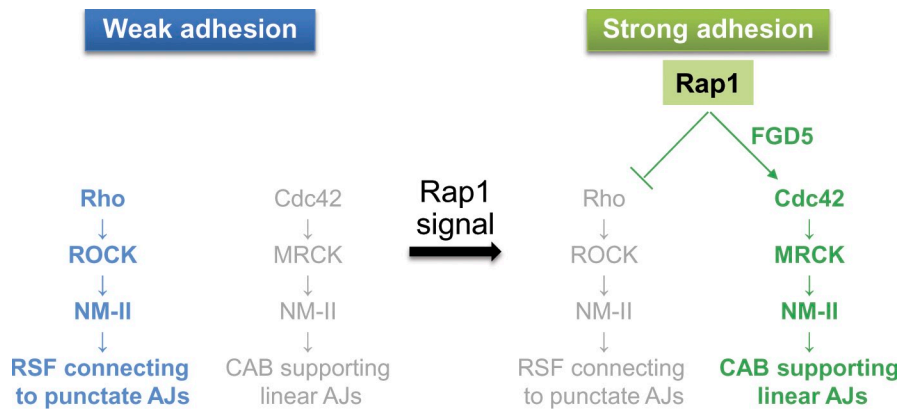
Weak adhesion

Strong adhesion

Rap1

FGD5

Rho → **ROCK** → **NM-II** → **RSF connecting to punctate AJs**

Cdc42 → MRCK → NM-II → CAB supporting linear AJs

Rap1 signal →

Rho → ROCK → NM-II → RSF connecting to punctate AJs

Cdc42 → **MRCK** → **NM-II** → **CAB supporting linear AJs**

Figure 9. **Schematic representation of the model that accounts for how Rap1 potentiates EC junctions.** In the ECs that establish weak cell–cell adhesions, the Rho–ROCK–NM-II pathway induces formation of RSF connecting to punctate AJs. Once activated, Rap1 induces disruption of RSF through inhibition of the Rho–ROCK–NM-II pathway and formation of CAB supporting linear AJs through activation of the Cdc42–MRCK–NM-II pathway, thereby potentiating EC junctions. Thus, Rap1 tunes the NM-II activity by regulating two Rho family GTPases to control EC junctions.

Biotechnology, Inc.; anti-FGD5 for immunocytochemistry (#HPA019191), anti–β-actin, and anti-FLAG (M2) from Sigma-Aldrich; rabbit anti-VE-cadherin, anti–NM-IIA, anti–NM-IIB, anti–phospho-RLC at Ser19 (#3671), anti–phospho-RLC at Thr18/Ser19 (#3678), anti-cAMP response element–binding protein (CREB), and anti–phospho-CREB at Ser133 from Cell Signaling Technology; anti-MRCKα from Abcam; anti-MRCKβ from Kazusa DNA Research Institute; anti-FGD5 for Western blotting (#H00152273) from Abnova; mouse and rabbit control IgG from Vector Laboratories; Alexa Fluor 488– or Alexa Fluor 633–labeled goat anti–mouse and anti–rabbit IgG from Invitrogen; and HRP-coupled goat anti–mouse and anti–rabbit IgG from GE Healthcare. Rhodamine-phalloidin was purchased from Invitrogen.

Plasmids

A cDNA fragment encoding human MRCKβ was obtained from Kazusa DNA Research Institute, and cloned into pEGFP-N1 vector (Takara Bio Inc.) to construct the pEGFP-N1-MRCKβ encoding MRCKβ with a C-terminal GFP tag (MRCKβ-GFP). pEGFP-N1-MRCKβ H1593/1596A plasmid encoding MRCKβ-GFP mutant in which His-1593 and His-1596 were replaced with Ala (MRCKβ H1593/1596A-GFP) was generated using a QuikChange site-directed mutagenesis kit (Agilent Technologies). A cDNA fragment encoding human Cdc42 was amplified by PCR, and subcloned into pEGFP-C1 and pmCherry-C1 vectors (Takara Bio Inc.) to generate the expression plasmids encoding Cdc42 with N-terminal GFP and mCherry tag, respectively. pERed-NLS expression plasmids encoding both wild-type or a constitutively active mutant of human RhoA, Rac1, or Cdc42 and IRES-driven NLS-tagged Express red were provided by M. Matsuda (Kyoto University, Kyoto, Japan; Aoki et al., 2005). pCXN2-EGFP-N-WASP CRIB plasmid, a gift from M. Matsuda, expresses CRIB domain of N-WASP with an N-terminal GFP tag (GFP-N-WASP). The expression vector encoding GFP-N-WASP mutant (GFP-N-WASP H211D) in which His-211 was replaced with Asp was generated using the QuikChange Site-directed mutagenesis kit. pCAGGS and pPBbsr vectors encoding a FRET biosensor for RhoA (Raichu-RhoA) and for Cdc42 (RaichuEV-Cdc42) were provided by M. Matsuda (Komatsu et al., 2011). In this study, we used modified RaichuEV-Cdc42 that contains the CAAX box of Cdc42 (amino acids 174–191) at the C terminus as a localization signal. A cDNA that encodes the amino acids 242–1,462 fragment of human FGD5 was purchased from Kazusa DNA Research Institute, and subcloned into pEGFP-C1 vector to construct pEGFP-C1-FGD5 (amino acids 242–1,462). To generate the plasmid encoding human FGD5 with an N-terminal GFP tag, a cDNA fragment encoding the N-terminal portion (amino acids 1–241) of human FGD5 was amplified by PCR using HUVEC cDNA as a template, and inserted into the site between GFP and FGD5 (242–1,462) in pEGFP-C1-FGD5 (242–1,462) vector. The siRNA-insensitive cDNA encoding MRCKβ-GFP, MRCKβ H1593/1596A-GFP, Cdc42, or FGD5 was generated using the QuikChange site-directed mutagenesis kit, and subcloned into pPBbsr vector (provided by M. Matsuda) for piggyBac transposon-mediated gene transfer (provided by A. Bradley, Wellcome Trust Sanger Institute, Cambridgeshire, England, UK; Yusa et al., 2009; Komatsu et al., 2011). pEGFP-N1-VE-cadherin plasmid encoding VE-cadherin C-terminally tagged with GFP (VE-cadherin-GFP) has already been described (Noda et al., 2010).

Cell culture, transfections, and siRNA-mediated protein knockdown

HUVECs were purchased from Kurabo, maintained in HuMedia-EG2 with a growth additive as described previously (Fukuhara et al., 2008), and used for the experiment before passage 7. 293T cells were cultured in Dulbecco's modified Eagle's medium (Nissui) supplemented with 10% fetal bovine serum and antibiotics (100 μg/ml streptomycin and 100 U/ml penicillin) as described previously (Fukuhara et al., 2008). HUVECs and 293T cells were transfected using Lipofectamine 2000 reagent (Invitrogen) and Lipofectamine Plus reagent (Invitrogen).

siRNAs targeting the genes indicated were purchased as follows: a mixture of siRNAs for NM-IIA and NM-IIB (#1, HSS106870 and HSS106873; #2, HSS106872 and HSS106875), MRCKα (HSS112351), MRCKβ (HSS114303), Cdc42 (#1, HSS101666; #2, HSS190761; #3, HSS190760), and FGD5 (#1, HSS135807; #2, HSS135806) from Invitrogen; a mixture of siRNAs for Rap1A and Rap1B (#1, J-003623-06-0005 and J-010364-07-0005; #2, J-003623-07-0005 and J-010364-06-0005; Pannekoek et al., 2011), and negative control siRNA (D-001810-10-05) from Thermo Fischer Scientific; and MRCK (5′-CGAGAAGACTTTGAAA-TAA-3′; Wilkinson et al., 2005) and negative control siRNA (SCI-001) from Sigma-Aldrich. HUVECs were transfected with siRNAs using Lipofectamine RNAi MAX reagent (Invitrogen). After 24 or 48 h of culture, the cells were replated, cultured for additional 24 h, and used for the experiments.

The piggyBac transposon system was used to generate mass cultures of HUVECs that express GFP, MRCKβ-GFP, MRCKβ H1593/1596A-GFP, Cdc42, or FGD5 (Yusa et al., 2009; Komatsu et al., 2011). HUVECs at passage 5 were transfected with pPBbsr vectors encoding the corresponding cDNA upstream of an IRES-blasticidin resistance cassette together with a plasmid expressing the piggyBac transposase. The cells were selected in the growth media containing 6 μg/ml blasticidin for 2 wk, expanded by replating into new dish, and used for the experiments.

Immunocytochemistry

Monolayer-cultured HUVECs grown on a 35-mm glass-base dish (Asahi Techno Glass) coated with Cellmatrix type I-C were starved in medium 199 (Invitrogen) containing 0.5% BSA, and stimulated with 10 μM FSK, 1 mM 007, or 0.5 mM 6-Bnz for 20 min. Immunocytochemistry was performed as described previously (Noda et al., 2010). After stimulation, the cells were fixed with PBS containing 2% formaldehyde for 30 min at 4°C, permeabilized with 0.05% Triton X-100 for 25 min at 4°C, and blocked with PBS containing 4% BSA for 1 h at RT. To detect Cdc42 expression, the cells were fixed with 10% trichloroacetic acid for 15 min at 4°C. The cells were immunostained with anti–VE-cadherin, anti–phospho-RLC at Ser19, anti–phospho-RLC at Thr18/Ser19, anti-Cdc42, anti-FGD5, and anti-FLAG antibodies at 4°C overnight. Protein reacting with antibody was visualized with species-matched Alexa Fluor 488– or Alexa Fluor 633–labeled secondary antibodies. To visualize F-actin, the cells were stained with rhodamine-phalloidin for 1 h at RT. Fluorescence images of GFP, mCherry, rhodamine, Alexa Fluor 488, and Alexa Fluor 633 were recorded with an inverted fluorescence microscope (IX-81; Olympus) with Plan-Apochromat 60×/1.40 NA and UPlan FL N 60×/1.25 NA oil immersion objective lenses (Olympus) and equipped with a pE-1 LED excitation system (CoolLED) with a cooled charge-coupled device camera (CoolSNAP HQ; Roper Scientific) or with a confocal microscope (FluoView FV1000; Olympus) with UPlan-SApochromat 60×/1.35 NA oil immersion objective lens (Olympus). The microscope and image acquisition were controlled by MetaMorph software (Universal Imaging) and FluoView ASW software (Olympus).

To quantify the amount of F-actin, phosphorylation of RLC, and FGD5 at the cell–cell junctions, their corresponding fluorescence intensities at the cell–cell contacts were measured using the line scan function in MetaMorph software (Universal Imaging). The 3-pixel-width lines were randomly drawn on the fluorescence images of the cells stained with rhodamine-phalloidin (rhodamine), and anti-pRLC (Alexa Fluor 488),

anti-FGD5 (Alexa Fluor 488), and anti–VE-cadherin (Alexa Fluor 633) antibodies. Then, the mean pixel intensity for each position along the line was determined by line scan analysis. The mean fluorescence intensity at the points across the cell–cell contacts defined by VE-cadherin fluorescence was scored as the amount of F-actin, phosphorylation of RLC, and FGD5 at the cell–cell contacts. For the rescue experiments (Fig. 3, F–H; and Fig. 6, B–D), the cell–cell junctions were defined by their morphological appearance in differential interference contrast images.

Detection of GTP-bound form of Rap1 and RhoA and phosphorylated CREB

To detect GTP-bound Rap1 and phosphorylated CREB, HUVECs were sequentially starved in 0.5% BSA-containing medium 199 for 3 h, and in 0.1% BSA-containing medium 199 for 1 h. The cells were then stimulated with vehicle, 10 µM FSK, 1 mM 007, or 0.5 mM 6-Bnz for 10 min. To detect GTP-bound RhoA, HUVECs were starved in 0.5% BSA-containing medium 199 for 4 h, and stimulated with either vehicle or 10 µM FSK for 20 min. GTP-bound forms of Rap1 and RhoA were assessed by performing a pull-down assay as described previously (Fukuhara et al., 2000, 2005). In brief, the cells were washed with cold PBS and lysed at 4°C in a pull-down lysis buffer containing 20 mM Tris-HCl, pH 7.5, 100 mM NaCl, 10 mM $MgCl_2$, 1% Triton X-100, 1 mM EGTA, 1 mM dithiothreitol, 1 mM Na_3VO_4, and protease inhibitor cocktail (Roche). Lysates were incubated with the glutathione transferase–tagged Rap1 binding domain of RalGDS or the Rho binding domain of Rhotekin precoupled to glutathione-Sepharose beads for 40 min at 4°C, followed by four washes with lysis buffer. GTP-bound Rap1 or GTP-bound RhoA were released from the beads by an addition of protein loading buffer, and subjected to Western blot analysis with anti-Rap1 or anti-RhoA antibody, respectively. Phosphorylation of CREB was determined by performing Western blot analysis with anti–phospho-CREB antibody as described previously (Fukuhara et al., 2005).

Immunoprecipitation

HUVECs stimulated with vehicle or FSK and 293T cells transfected with plasmids indicated in figure legends were lysed at 4°C in lysis buffer containing 20 mM Tris-HCl, pH 7.5, 100 mM NaCl, 10 mM $MgCl_2$, 1% Triton X-100, 1 mM EGTA, 1 mM Na_3Vo_4, and 1× protease inhibitor cocktail (Roche), centrifuged at 17,400 rpm for 15 min, and incubated with anti–NM-II and anti-FLAG antibodies for 3 h at 4°C, respectively. Immunoprecipitates collected on protein G–Sepharose beads (GE Healthcare) and aliquots of total cellular lysates were subjected to Western blot analysis with anti–NM-II, anti-MRCK, anti-FLAG, and anti-GFP antibodies.

Time-lapse fluorescence imaging

To visualize activities of RhoA and Cdc42 in living cells, FRET imaging was performed as described previously (Sakurai et al., 2006). In brief, HUVECs transfected with a plasmid encoding Rahicu-RhoA or RaichuEV-Cdc42 were plated at confluent density on a collagen-coated glass base dish, cultured overnight, starved in phenol red–free medium 199 containing 0.5% BSA for 3 h, and stimulated with vehicle, 10 µM FSK, or 1 mM 007 at 37°C with 5% CO_2 using a heating chamber (Tokai Hit). The cells were imaged every 2 min with an inverted fluorescence microscope (IX-81) equipped with a Plan-Apochromat 60×/1.40 NA oil immersion objective lens, a cooled charge-coupled device camera (CoolSNAP HQ), and a pE-1 LED excitation system. Dual images for CFP and YFP were obtained through an XF1071 excitation filter, a XF2034 dichroic mirror, and an XF3075 emission filter for CFP and an XF 3079 emission filter for YFP (Omega Scientific, Inc.), respectively. After background subtraction, the FRET/CFP ratio images were created by MetaMorph software (Molecular Devices) and displayed as an intensity-modulated display image. For quantitative FRET analysis, the FRET/CFP ratio of each cell was calculated by dividing the fluorescence intensity of YFP by that of CFP in total cellular area. Relative values of FRET/CFP were calculated by the value of FRET/CFP ratio induced by FSK or 007 divided by that induced by vehicle at the corresponding time points.

HUVECs expressing GFP- or mCherry-tagged proteins were time-lapse imaged similar to FRET imaging. All experiments were performed at 37°C with 5% CO_2 using a heating chamber.

Fluorescence recovery after photobleaching analysis

FRAP analysis was performed on a confocal laser-scanning microscope (FluoView FV1000) with a UPlan-SApochromat 60×/1.35 NA oil immersion objective lens and equipped with photomultiplier tubes regulated by Fluoview ASW software, as described previously (Noda et al., 2010). In brief, HUVECs plated on collagen-coated dish were transfected with the plasmid encoding VE-cadherin-GFP, starved in medium 199 containing 0.5%

BSA, and stimulated with 10 µM FSK at 37°C. GFP-positive cells surrounded by GFP-negative cells were selected and subjected to FRAP analysis. GFP molecules were excited with the 488-nm line from an Argon ion laser. 20 min after stimulation, GFP fluorescence at the region of cell–cell contacts (a 13-µm-diameter circle) was bleached using the SIM scanner in tornado scan mode with the 405-nm diode laser set at full power for 5 s. Less than 5% of total fluorescence was lost during the bleaching. To monitor fluorescence recovery, images were acquired every 60 s over a period 50–60 min. Using Excel software (Microsoft), data were corrected for the overall loss in total fluorescence intensity as a result of the imaging scans. The fluorescence intensity of the bleached region over time was normalized with the mean fluorescence intensity before bleaching. Recovery measurements were quantified by fitting normalized fluorescence intensities of bleached areas to a one-phase exponential association using Prism 5 software (GraphPad Software).

Impedance measurement by ECIS

Barrier function of EC junctions was evaluated by using ECIS-zθ (Applied Biophysics) as described previously (Lo et al., 1999; Pannekoek et al., 2011). In brief, 10^5 HUVECs were plated on collagen-coated 8W10E electrodes and cultured overnight. Then, the cells were starved in 0.5% BSA-containing medium 199 for 4 h, and subjected to the ECIS measurement. Rb was measured in real time at 37°C with 5% CO_2 in a CO_2 incubator using a ECIS-zθ system at 4,000, 16,000, and 64,000 Hz.

Permeability assay

Permeability across the HUVEC monolayer was measured by using a collagen-coated transwell unit (6.5 mm in diameter, 3.0-µm pore size polycarbonate filter; Corning) as described previously (Fukuhara et al., 2005). To examine the effect of blebbistatin on EC permeability, HUVECs (10^5 cells) were plated in the upper chamber of the transwell, and cultured for 3 d. The cells were then treated with either vehicle or 20 µM blebbistatin for 4 h, and stimulated with either vehicle or 10 mM FSK in the presence or absence of blebbistatin for 30 min. To examine the effect of depletion of MRCK, the HUVECs transfected with MRCK siRNA were plated in the upper chamber of the transwell, cultured for 1 d, and used for the experiments, as MRCK expression was recovered by 3 d after the siRNA transfection. Then, permeability was measured by replacing the media in the upper chamber with media containing 1 mg/ml FITC-labeled dextran (mol wt 3,000). Similarly, permeability across the monolayer of HUVEC transfected with either control or MRCK siRNA was also measured.

Statistical analysis

Data are expressed as mean ± SEM. Statistical significance was determined by a Student's t test for paired samples or one-way analysis of variance with Turkey's test for multiple comparisons. Data were considered statistically significant if $P < 0.05$.

Online supplemental material

Fig. S1 shows that Rap1 induces RLC phosphorylation and CAB formation at cell–cell contacts. Fig. S2 shows the requirement of MRCK for Rap1-induced phosphorylation of RLC and formation of CAB at cell–cell junctions. Fig. S3 shows the involvement of Cdc42 in Rap1-induced CAB formation. Fig. S4 shows that FGD5 is required for Rap1-induced CAB formation. Fig. S5 shows that Rap1 potentiates EC junctions through FGD5–Cdc42–MRCK–NM-II–mediated CAB formation. Online supplemental material is available at http://www.jcb.org/cgi/content/full/jcb.201301115/DC1.

References

Abraham, S., M. Yeo, M. Montero-Balaguer, H. Paterson, E. Dejana, C.J. Marshall, and G. Mavria. 2009. VE-Cadherin-mediated cell-cell interaction suppresses sprouting via signaling to MLC2 phosphorylation. *Curr. Biol.* 19:668–674. http://dx.doi.org/10.1016/j.cub.2009.02.057

Aoki, K., T. Nakamura, K. Fujikawa, and M. Matsuda. 2005. Local phosphatidylinositol 3,4,5-trisphosphate accumulation recruits Vav2 and Vav3 to activate Rac1/Cdc42 and initiate neurite outgrowth in nerve growth factor-stimulated PC12 cells. *Mol. Biol. Cell.* 16:2207–2217. http://dx.doi.org/10.1091/mbc.E04-10-0904

Augustin, H.G., G.Y. Koh, G. Thurston, and K. Alitalo. 2009. Control of vascular morphogenesis and homeostasis through the angiopoietin-Tie system. *Nat. Rev. Mol. Cell Biol.* 10:165–177. http://dx.doi.org/10.1038/nrm2639

Ayollo, D.V., I.Y. Zhitnyak, J.M. Vasiliev, and N.A. Gloushankova. 2009. Rearrangements of the actin cytoskeleton and E-cadherin-based adherens junctions caused by neoplasic transformation change cell-cell interactions. *PLoS ONE.* 4:e8027. http://dx.doi.org/10.1371/journal.pone.0008027

Borikova, A.L., C.F. Dibble, N. Sciaky, C.M. Welch, A.N. Abell, S. Bencharit, and G.L. Johnson. 2010. Rho kinase inhibition rescues the endothelial cell cerebral cavernous malformation phenotype. *J. Biol. Chem.* 285:11760–11764. http://dx.doi.org/10.1074/jbc.C109.097220

Broman, M.T., D. Mehta, and A.B. Malik. 2007. Cdc42 regulates the restoration of endothelial adherens junctions and permeability. *Trends Cardiovasc. Med.* 17:151–156. http://dx.doi.org/10.1016/j.tcm.2007.03.004

Cheng, C., R. Haasdijk, D. Tempel, E.H.M. van de Kamp, R. Herpers, F. Bos, W.K. Den Dekker, L.A.J. Blonden, R. de Jong, P.E. Bürgisser, et al. 2012. Endothelial cell-specific FGD5 involvement in vascular pruning defines neovessel fate in mice. *Circulation.* 125:3142–3158. http://dx.doi.org/10.1161/CIRCULATIONAHA.111.064030

Chew, T.L., R.A. Masaracchia, Z.M. Goeckeler, and R.B. Wysolmerski. 1998. Phosphorylation of non-muscle myosin II regulatory light chain by p21-activated kinase (gamma-PAK). *J. Muscle Res. Cell Motil.* 19:839–854. http://dx.doi.org/10.1023/A:1005417926585

Cullere, X., S.K. Shaw, L. Andersson, J. Hirahashi, F.W. Luscinskas, and T.N. Mayadas. 2005. Regulation of vascular endothelial barrier function by Epac, a cAMP-activated exchange factor for Rap GTPase. *Blood.* 105:1950–1955. http://dx.doi.org/10.1182/blood-2004-05-1987

Dejana, E., F. Orsenigo, and M.G. Lampugnani. 2008. The role of adherens junctions and VE-cadherin in the control of vascular permeability. *J. Cell Sci.* 121:2115–2122. http://dx.doi.org/10.1242/jcs.017897

Fukuhara, S., H. Chikumi, and J.S. Gutkind. 2000. Leukemia-associated Rho guanine nucleotide exchange factor (LARG) links heterotrimeric G proteins of the G(12) family to Rho. *FEBS Lett.* 485:183–188. http://dx.doi.org/10.1016/S0014-5793(00)02224-9

Fukuhara, S., K. Shimizu, T. Kawakatsu, T. Fukuyama, Y. Minami, T. Honda, T. Hoshino, T. Yamada, H. Ogita, M. Okada, and Y. Takai. 2004. Activation of Cdc42 by trans interactions of the cell adhesion molecules nectins through c-Src and Cdc42-GEF FRG. *J. Cell Biol.* 166:393–405. http://dx.doi.org/10.1083/jcb.200401093

Fukuhara, S., A. Sakurai, H. Sano, A. Yamagishi, S. Somekawa, N. Takakura, Y. Saito, K. Kangawa, and N. Mochizuki. 2005. Cyclic AMP potentiates vascular endothelial cadherin-mediated cell-cell contact to enhance endothelial barrier function through an Epac-Rap1 signaling pathway. *Mol. Cell. Biol.* 25:136–146. http://dx.doi.org/10.1128/MCB.25.1.136-146.2005

Fukuhara, S., K. Sako, T. Minami, K. Noda, H.Z. Kim, T. Kodama, M. Shibuya, N. Takakura, G.Y. Koh, and N. Mochizuki. 2008. Differential function of Tie2 at cell-cell contacts and cell-substratum contacts regulated by angiopoietin-1. *Nat. Cell Biol.* 10:513–526. http://dx.doi.org/10.1038/ncb1714

Fukuhra, S., A. Sakurai, A. Yamagishi, K. Sako, and N. Mochizuki. 2006. Vascular endothelial cadherin-mediated cell-cell adhesion regulated by a small GTPase, Rap1. *J. Biochem. Mol. Biol.* 39:132–139. http://dx.doi.org/10.5483/BMBRep.2006.39.2.132

Fukuyama, T., H. Ogita, T. Kawakatsu, T. Fukuhara, T. Yamada, T. Sato, K. Shimizu, T. Nakamura, M. Matsuda, and Y. Takai. 2005. Involvement of the c-Src-Crk-C3G-Rap1 signaling in the nectin-induced activation of Cdc42 and formation of adherens junctions. *J. Biol. Chem.* 280:815–825.

Gaggioli, C., S. Hooper, C. Hidalgo-Carcedo, R. Grosse, J.F. Marshall, K. Harrington, and E. Sahai. 2007. Fibroblast-led collective invasion of carcinoma cells with differing roles for RhoGTPases in leading and following cells. *Nat. Cell Biol.* 9:1392–1400. http://dx.doi.org/10.1038/ncb1658

Garcia, J.G., F. Liu, A.D. Verin, A. Birukova, M.A. Dechert, W.T. Gerthoffer, J.R. Bamberg, and D. English. 2001. Sphingosine 1-phosphate promotes endothelial cell barrier integrity by Edg-dependent cytoskeletal rearrangement. *J. Clin. Invest.* 108:689–701.

Gavard, J., and J.S. Gutkind. 2006. VEGF controls endothelial-cell permeability by promoting the beta-arrestin-dependent endocytosis of VE-cadherin. *Nat. Cell Biol.* 8:1223–1234. http://dx.doi.org/10.1038/ncb1486

Glading, A., J. Han, R.A. Stockton, and M.H. Ginsberg. 2007. KRIT-1/CCM1 is a Rap1 effector that regulates endothelial cell–cell junctions. *J. Cell Biol.* 179:247–254. http://dx.doi.org/10.1083/jcb.200705175

Gomes, E.R., S. Jani, and G.G. Gundersen. 2005. Nuclear movement regulated by Cdc42, MRCK, myosin, and actin flow establishes MTOC polarization in migrating cells. *Cell.* 121:451–463. http://dx.doi.org/10.1016/j.cell.2005.02.022

Gomez, G.A., R.W. McLachlan, and A.S. Yap. 2011. Productive tension: force-sensing and homeostasis of cell-cell junctions. *Trends Cell Biol.* 21:499–505. http://dx.doi.org/10.1016/j.tcb.2011.05.006

Hoelzle, M.K., and T. Svitkina. 2012. The cytoskeletal mechanisms of cell-cell junction formation in endothelial cells. *Mol. Biol. Cell.* 23:310–323. http://dx.doi.org/10.1091/mbc.E11-08-0719

Hogan, C., N. Serpente, P. Cogram, C.R. Hosking, C.U. Bialucha, S.M. Feller, V.M. Braga, W. Birchmeier, and Y. Fujita. 2004. Rap1 regulates the formation of E-cadherin-based cell-cell contacts. *Mol. Cell. Biol.* 24:6690–6700. http://dx.doi.org/10.1128/MCB.24.15.6690-6700.2004

Huveneers, S., J. Oldenburg, E. Spanjaard, G. van der Krogt, I. Grigoriev, A. Akhmanova, H. Rehmann, and J. de Rooij. 2012. Vinculin associates with endothelial VE-cadherin junctions to control force-dependent remodeling. *J. Cell Biol.* 196:641–652. http://dx.doi.org/10.1083/jcb.201108120

Ikebe, M., and D.J. Hartshorne. 1985. Phosphorylation of smooth muscle myosin at two distinct sites by myosin light chain kinase. *J. Biol. Chem.* 260:10027–10031.

Knox, A.L., and N.H. Brown. 2002. Rap1 GTPase regulation of adherens junction positioning and cell adhesion. *Science.* 295:1285–1288. http://dx.doi.org/10.1126/science.1067549

Komatsu, N., K. Aoki, M. Yamada, H. Yukinaga, Y. Fujita, Y. Kamioka, and M. Matsuda. 2011. Development of an optimized backbone of FRET biosensors for kinases and GTPases. *Mol. Biol. Cell.* 22:4647–4656. http://dx.doi.org/10.1091/mbc.E11-01-0072

Kooistra, M.R., M. Corada, E. Dejana, and J.L. Bos. 2005. Epac1 regulates integrity of endothelial cell junctions through VE-cadherin. *FEBS Lett.* 579:4966–4972. http://dx.doi.org/10.1016/j.febslet.2005.07.080

Kurogane, Y., M. Miyata, Y. Kubo, Y. Nagamatsu, R.K. Kundu, A. Uemura, T. Ishida, T. Quertermous, K. Hirata, and Y. Rikitake. 2012. FGD5 mediates proangiogenic action of vascular endothelial growth factor in human vascular endothelial cells. *Arterioscler. Thromb. Vasc. Biol.* 32:988–996. http://dx.doi.org/10.1161/ATVBAHA.111.244004

Leung, T., X.Q. Chen, I. Tan, E. Manser, and L. Lim. 1998. Myotonic dystrophy kinase-related Cdc42-binding kinase acts as a Cdc42 effector in promoting cytoskeletal reorganization. *Mol. Cell. Biol.* 18:130–140.

Lo, C.M., C.R. Keese, and I. Giaever. 1999. Cell-substrate contact: another factor may influence transepithelial electrical resistance of cell layers cultured on permeable filters. *Exp. Cell Res.* 250:576–580. http://dx.doi.org/10.1006/excr.1999.4538

Millán, J., R.J. Cain, N. Reglero-Real, C. Bigarella, B. Marcos-Ramiro, L. Fernández-Martín, I. Correas, and A.J. Ridley. 2010. Adherens junctions connect stress fibres between adjacent endothelial cells. *BMC Biol.* 8:11. http://dx.doi.org/10.1186/1741-7007-8-11

Nakhaei-Nejad, M., G. Haddad, Q.X. Zhang, and A.G. Murray. 2012. Facio-genital dysplasia-5 regulates matrix adhesion and survival of human endothelial cells. *Arterioscler. Thromb. Vasc. Biol.* 32:2694–2701. http://dx.doi.org/10.1161/ATVBAHA.112.300074

Noda, K., J. Zhang, S. Fukuhara, S. Kunimoto, M. Yoshimura, and N. Mochizuki. 2010. Vascular endothelial-cadherin stabilizes at cell-cell junctions by anchoring to circumferential actin bundles through alpha-and beta-catenins in cyclic AMP-Epac-Rap1 signal-activated endothelial cells. *Mol. Biol. Cell.* 21:584–596. http://dx.doi.org/10.1091/mbc.E09-07-0580

Otani, T., T. Ichii, S. Aono, and M. Takeichi. 2006. Cdc42 GEF Tuba regulates the junctional configuration of simple epithelial cells. *J. Cell Biol.* 175:135–146. http://dx.doi.org/10.1083/jcb.200605012

Pannekoek, W.J., J.J.G. van Dijk, O.Y. Chan, S. Huveneers, J.R. Linnemann, E. Spanjaard, P.M. Brouwer, A.J. van der Meer, F.J.T. Zwartkruis, H. Rehmann, et al. 2011. Epac1 and PDZ-GEF cooperate in Rap1 mediated endothelial junction control. *Cell. Signal.* 23:2056–2064. http://dx.doi.org/10.1016/j.cellsig.2011.07.022

Price, L.S., A. Hajdo-Milasinovic, J. Zhao, F.J. Zwartkruis, J.G. Collard, and J.L. Bos. 2004. Rap1 regulates E-cadherin-mediated cell-cell adhesion. *J. Biol. Chem.* 279:35127–35132. http://dx.doi.org/10.1074/jbc.M404917200

Ramchandran, R., D. Mehta, S.M. Vogel, M.K. Mirza, P. Kouklis, and A.B. Malik. 2008. Critical role of Cdc42 in mediating endothelial barrier

protection in vivo. *Am. J. Physiol. Lung Cell. Mol. Physiol.* 295:L363–L369. http://dx.doi.org/10.1152/ajplung.90241.2008

Ratheesh, A., and A.S. Yap. 2012. A bigger picture: classical cadherins and the dynamic actin cytoskeleton. *Nat. Rev. Mol. Cell Biol.* 13:673–679. http://dx.doi.org/10.1038/nrm3431

Sakurai, A., S. Fukuhara, A. Yamagishi, K. Sako, Y. Kamioka, M. Masuda, Y. Nakaoka, and N. Mochizuki. 2006. MAGI-1 is required for Rap1 activation upon cell-cell contact and for enhancement of vascular endothelial cadherin-mediated cell adhesion. *Mol. Biol. Cell.* 17:966–976. http://dx.doi.org/10.1091/mbc.E05-07-0647

Sanders, L.C., F. Matsumura, G.M. Bokoch, and P. de Lanerolle. 1999. Inhibition of myosin light chain kinase by p21-activated kinase. *Science.* 283:2083–2085. http://dx.doi.org/10.1126/science.283.5410.2083

Smutny, M., H.L. Cox, J.M. Leerberg, E.M. Kovacs, M.A. Conti, C. Ferguson, N.A. Hamilton, R.G. Parton, R.S. Adelstein, and A.S. Yap. 2010. Myosin II isoforms identify distinct functional modules that support integrity of the epithelial zonula adherens. *Nat. Cell Biol.* 12:696–702. http://dx.doi.org/10.1038/ncb2072

Stockton, R.A., E. Schaefer, and M.A. Schwartz. 2004. p21-activated kinase regulates endothelial permeability through modulation of contractility. *J. Biol. Chem.* 279:46621–46630. http://dx.doi.org/10.1074/jbc.M408877200

Stockton, R.A., R. Shenkar, I.A. Awad, and M.H. Ginsberg. 2010. Cerebral cavernous malformations proteins inhibit Rho kinase to stabilize vascular integrity. *J. Exp. Med.* 207:881–896. http://dx.doi.org/10.1084/jem.20091258

Taguchi, K., T. Ishiuchi, and M. Takeichi. 2011. Mechanosensitive EPLIN-dependent remodeling of adherens junctions regulates epithelial reshaping. *J. Cell Biol.* 194:643–656. http://dx.doi.org/10.1083/jcb.201104124

Tan, I., K.T. Seow, L. Lim, and T. Leung. 2001. Intermolecular and intramolecular interactions regulate catalytic activity of myotonic dystrophy kinase-related Cdc42-binding kinase alpha. *Mol. Cell. Biol.* 21:2767–2778. http://dx.doi.org/10.1128/MCB.21.8.2767-2778.2001

Tan, I., J. Yong, J.M. Dong, L. Lim, and T. Leung. 2008. A tripartite complex containing MRCK modulates lamellar actomyosin retrograde flow. *Cell.* 135:123–136. http://dx.doi.org/10.1016/j.cell.2008.09.018

Tan, I., J. Lai, J. Yong, S.F. Li, and T. Leung. 2011. Chelerythrine perturbs lamellar actomyosin filaments by selective inhibition of myotonic dystrophy kinase-related Cdc42-binding kinase. *FEBS Lett.* 585:1260–1268. http://dx.doi.org/10.1016/j.febslet.2011.03.054

Vicente-Manzanares, M., X. Ma, R.S. Adelstein, and A.R. Horwitz. 2009. Non-muscle myosin II takes centre stage in cell adhesion and migration. *Nat. Rev. Mol. Cell Biol.* 10:778–790. http://dx.doi.org/10.1038/nrm2786

Wilkinson, S., H.F. Paterson, and C.J. Marshall. 2005. Cdc42-MRCK and Rho-ROCK signalling cooperate in myosin phosphorylation and cell invasion. *Nat. Cell Biol.* 7:255–261. http://dx.doi.org/10.1038/ncb1230

Wimmer, R., B. Cseh, B. Maier, K. Scherrer, and M. Baccarini. 2012. Angiogenic sprouting requires the fine tuning of endothelial cell cohesion by the Raf-1/Rok-α complex. *Dev. Cell.* 22:158–171. http://dx.doi.org/10.1016/j.devcel.2011.11.012

Wirth, A., M. Schroeter, C. Kock-Hauser, E. Manser, J.M. Chalovich, P. De Lanerolle, and G. Pfitzer. 2003. Inhibition of contraction and myosin light chain phosphorylation in guinea-pig smooth muscle by p21-activated kinase 1. *J. Physiol.* 549:489–500. http://dx.doi.org/10.1113/jphysiol.2002.033167

Wittchen, E.S., R.A. Worthylake, P. Kelly, P.J. Casey, L.A. Quilliam, and K. Burridge. 2005. Rap1 GTPase inhibits leukocyte transmigration by promoting endothelial barrier function. *J. Biol. Chem.* 280:11675–11682. http://dx.doi.org/10.1074/jbc.M412595200

Yamamoto, M., S.H. Ramirez, S. Sato, T. Kiyota, R.L. Cerny, K. Kaibuchi, Y. Persidsky, and T. Ikezu. 2008. Phosphorylation of claudin-5 and occludin by rho kinase in brain endothelial cells. *Am. J. Pathol.* 172:521–533. http://dx.doi.org/10.2353/ajpath.2008.070076

Yamashiro, S., G. Totsukawa, Y. Yamakita, Y. Sasaki, P. Madaule, T. Ishizaki, S. Narumiya, and F. Matsumura. 2003. Citron kinase, a Rho-dependent kinase, induces di-phosphorylation of regulatory light chain of myosin II. *Mol. Biol. Cell.* 14:1745–1756. http://dx.doi.org/10.1091/mbc.E02-07-0427

Yoneda, A., H.A.B. Multhaupt, and J.R. Couchman. 2005. The Rho kinases I and II regulate different aspects of myosin II activity. *J. Cell Biol.* 170:443–453. http://dx.doi.org/10.1083/jcb.200412043

Yusa, K., R. Rad, J. Takeda, and A. Bradley. 2009. Generation of transgene-free induced pluripotent mouse stem cells by the piggyBac transposon. *Nat. Methods.* 6:363–369. http://dx.doi.org/10.1038/nmeth.1323

Zeng, Q., D. Lagunoff, R. Masaracchia, Z. Goeckeler, G. Côté, and R. Wysolmerski. 2000. Endothelial cell retraction is induced by PAK2 monophosphorylation of myosin II. *J. Cell Sci.* 113:471–482.